A DYNAMIC ANALYSIS
OF THE
OKANAGAN LAKE FLOATING BRIDGE

by

ERIC R. MORRIS

B.A.Sc., University of British Columbia, 1997

A THESIS SUBMITTED IN PARTIAL FULFILMENT OF
THE REQUIREMENTS FOR THE DEGREE OF
MASTER OF APPLIED SCIENCE

in

THE FACULTY OF GRADUATE STUDIES

Department of Civil Engineering

We accept this thesis as conforming
to the required standard

THE UNIVERSITY OF BRITISH COLUMBIA

October 1999

In presenting this thesis in partial fulfilment of the requirements for an advanced degree at the University of British Columbia, I agree that the Library shall make it freely available for reference and study. I further agree that permission for extensive copying of this thesis for scholarly purposes may be granted by the head of my department or by his or her representatives. It is understood that copying or publication of this thesis for financial gain shall not be allowed without my written permission.

Department of CIVIL ENGINEERING

The University of British Columbia
Vancouver, Canada

Date OCTOBER 4, 1999

DE-6 (2/88)

ABSTRACT

This thesis describes a time domain dynamic analysis of a proposed floating bridge on Okanagan Lake in Kelowna, British Columbia, Canada. The analysis begins with wave hindcasting using wind data collected at the bridge site and the nearby towns of Penticton and Kelowna. The influence of lake geometry and bathymetry on the design wave conditions is accounted for through the use of a numerical wave hindcasting model. The results of the wave hindcasting model are compared with wave data collected at the bridge site, and directional wave spectra based on the design wave conditions are then constructed for north and south storms.

The next stage of the analysis is the calculation of wave loads on the bridge. A computer model based on two-dimensional linear wave diffraction theory is used to calculate the sectional hydrodynamic coefficients. Force time series are then computed by discretizing the directional wave spectra, and combining the regular wave components with the appropriate wave exciting force coefficients and random phases. Superposition of these forces provides the hydrodynamic forces on the bridge as a function of time.

A structural analysis of the bridge based on the finite element method is then conducted for north and south storms. The results of the analysis include sway, heave and roll displacements, bending moments in the pontoons and mooring cable tensions. Additional topics that are investigated include the influence of slowly-varying wave drift forces on the response of the bridge, and the variability in response parameters between simulations.

The south storm was found to provide the largest bridge response with maximum bending moments about the z and y axes of the pontoon string of 190,000 and 290,000

kNm respectively, and a maximum cable tension of 1,670 kN. Variability between simulations was found to be considerable, with an average coefficient of variability of 0.096 for all response parameters in 10 simulations. The slowly-varying wave drift force was found to be equivalent to a static wave drift force at the significant wave height.

TABLE OF CONTENTS

LIST OF TABLES

LIST OF FIGURES

ACKNOWLEDGEMENTS

The author wishes to thank Dr. Michael Isaacson for his guidance and advice. In addition, the author wishes to thank Westmar Consultants Inc. for the opportunity to work on this project, and in particular William Kendrick, whose encyclopedic knowledge of the Okanagan Lake Floating Bridge proved invaluable during the preparation of this thesis.

Financial support in the form of a post-graduate scholarship from the Natural Sciences and Engineering Research Council of Canada is gratefully acknowledged.

1. INTRODUCTION

1.1 DYNAMIC ANALYSIS OF FLOATING BRIDGES

Floating bridges have been used in civil and military applications for centuries. Some of the advantages of floating bridges include ease of construction and comparatively low cost. Given these advantages, one might expect floating bridges to be an integral part of many countries' infrastructure. Today, however, few floating bridges exist in the world, with the greatest concentration of floating bridges found in the Pacific Northwest of North America. The Okanagan Lake Floating Bridge in Kelowna, British Columbia, Canada, is one of five floating bridges in this region.

Floating bridges have usually found modern application in situations where conventional bridge designs have proven unworkable. Because floating bridges derive vertical support from their own buoyancy, they can be used in locations were the body of water being crossed is too deep to economically construct bridge piers. Similarly, floating bridges can be used in locations where the soil conditions are unsuitable for bridge pier foundations.

Most modern floating bridges use concrete or steel pontoons connected together to form the bridge deck. The roadway is either laid directly on the pontoons or is placed on an elevated structure founded on the pontoons. Two distinct methods have been used to give floating bridges lateral stability. One method is to moor the bridge with pre-stressed cables attached to anchors on the seabed. Another method is to curve the bridge and gain lateral stability from arch action. The latter method is suitable only in locations where strong foundation material exists to provide support reactions. Examples of arched and moored floating bridges are presented in Figures 1 and 2.

Perhaps the greatest barrier to more widespread use of floating bridges is a lack of understanding of their behavior under environmental loads. The primary sources of environmental loading on a floating bridge are wind, ice and waves. The wind and ice loading problems are relatively well understood; however, the wave loading problem has only recently become tractable.

Traditional analyses of floating structures consider the wave field to be random and unidirectional. In reality, a wind generated sea is composed of wave trains with numerous frequencies and directions. When superposed, these wave trains add and cancel, producing a wave field in which the wave crests are of random and finite length. This type of sea surface is termed a short-crested wave field.

Modeling a wave field as random and unidirectional has proven acceptable for the analysis of structures whose dimensions are small compared to the wavelength of the incident waves. However, if one were to analyze the behavior of a long floating structure, such as a floating bridge, subject to infinite crested, random waves, unrealistically large loads and stresses would be predicted. These large loads and stresses are the result of the high degree of correlation of the forces along the bridge span. When the wave field is modeled as short-crested, the forces along the bridge span become uncorrelated, and the response of the bridge is reduced to levels more commonly observed in nature. As a result, the short-crestedness of the wave field, or what are termed directional wave effects must be considered for the safe, economical design of long floating structures.

The dynamic response of floating bridges to wave action can be determined in either the frequency or time domain. In a frequency domain approach, the directional

wave spectrum is determined, the frequency dependent hydrodynamic coefficients are calculated, and then exciting force spectra are derived. A structural model of the bridge is then created, and response spectra for parameters of interest such as cable forces and bending moments are created. The exciting force spectra are then combined with the response spectra to produce spectra of cables forces and bending moments. Statistical methods are then applied to determine the maximum forces in the bridge, which are exceeded with some desired probability.

In a time domain approach, time histories of wave force are synthesized from the directional wave spectrum and force coefficients. These force time histories are then applied to the structural model of the bridge and the response of the bridge is determined as a function of time. The maximum cable forces and bending moments that occur during the simulation are then determined by examining the response of the bridge at each time step.

Both solution techniques have advantages and disadvantages. The frequency domain approach can only be used with linear systems, and although the maximum forces and displacements can be determined with confidence, one cannot easily obtain a coincident set of forces. This is a considerable disadvantage during structural design since the stresses within a member depend critically on the combination of axial load and vertical, horizontal and torsional moments applied.

Time domain dynamic analysis can be applied to non-linear systems, and coincident forces are easily obtained from the time-history output. The major disadvantage of the time domain approach is that the results are variable. The forces and displacements obtained during a simulation depend critically on the set of random phases

selected when synthesizing the force time histories. As a result, the maximum forces obtained in each simulation will be different, and a single simulation may not provide a representative design value. This shortcoming can be overcome by performing several simulations with different random phases. The output of the simulations can then be treated as a set of samples from which the population statistics must be estimated.

In this thesis, a time domain dynamic analysis of a proposed four-lane replacement for the Okanagan Lake Floating Bridge is conducted. The variability in the output results is examined, and a technique for estimating population statistics from the results of a series of time domain simulations is proposed. In addition, a slowly-varying wave drift force is included in the analysis, and its influence on the response of the bridge is investigated.

1.2 LITERATURE REVIEW

1.2.1 EXTREME VALUE ESTIMATION

Estimating the magnitude of extreme events is a common task in many branches of civil engineering. In coastal and ocean engineering, extreme value estimation is applied to wind and waves. Structures are generally designed to resist an event that has a specified probability of occurring over the life of the structure. Load and resistance safety factors are then applied in structural design to bring the probability of failure to an acceptable level.

In most circumstances, wind and wave data is not available over a duration comparable with the design life of a structure, and therefore a suitable extrapolation is necessary. In addition, it is common that not enough data is available to obtain the parent

probability distribution of the wind or waves with accuracy, particularly for small probabilities of occurrence.

Gumbel (1958) observed that the parent probability distributions of many variables tends to three asymptotic forms for large return period events. These limiting forms are a double exponential form and two single exponential forms. The double exponential form is known as both the Gumbel and Type I distribution, and was originally researched by Fisher and Tippett (1928).

The Type I distribution is convenient to apply, and has been shown to provide reliable results in many applications ranging from flood prediction to extreme wind estimation. For this reason, the Type I distribution has been used for extreme wind estimation in this thesis.

1.2.2 ESTIMATION OF WAVE STATISTICS

Wave Statistics from Wind Data

The estimation of wave statistics from wind data is termed wave hindcasting. Wave hindcasting is often necessary because long, statistically significant records of wave data are rarely available. Wave hindcasting procedures can generally be divided into two categories:

- significant wave methods;
- wind field methods.

The significant wave method is the most widely applied technique for determining the characteristics of a wave field from wind data. Significant wave techniques were developed by Sverdrup and Munk (1947) and Bretschneider (1958).

These researchers related wind parameters such as speed, duration and fetch length to characteristic wave parameters (the significant wave height and peak period) and created empirical wave hindcasting curves for this purpose. Bretschneider (1961) also derived a wave spectrum that is defined in terms of the significant wave height and peak wave period.

Wind field methods relate the wind velocity directly to the wave spectrum. Wave spectra that use this approach include the Pierson-Moscowitz Spectrum (1964) and the JONSWAP spectrum derived by Hasselmann et al. (1973).

An important advance in wave hindcasting was the numerical implementation of wind field methods. Numerical models have been developed which can account for temporal and spatial variations in the wind field, limited fetch and duration, wave short-crestedness, refraction, wave breaking and bottom friction.

One of the first numerical wave hindcasting models was developed by Cardone, Pierson and Ward (1976). Their model was specifically designed to model duration limited hurricane generated waves, and was calibrated with historical data. Contributions to the development of computerized wave hindcasting models were also made by Barnett (1968), Inoue (1967), and Pierson et al. (1966).

More recently, a numerical wind field method was developed by Holthuijsen, Booij and Herbers (1989). Their model is stationary, and determines the directional wave spectrum from the wind field at a series of grid locations based on a numerical integration of the wave action balance equation. The model accounts for wave generation by wind, energy losses due to wave breaking and bottom friction, refraction, and wave-current interaction. This model forms the basis of the MIKE 21 Nearshore Spectral Wind Wave

Program that has been used for wave hindcasting in this thesis. This computer program is distributed and developed by the Danish Hydraulic Institute in Denmark.

The numerical wave hindcasting techniques described above rely upon a mathematical description of wave generation by wind. The mechanisms of wave generation by wind are not yet fully understood; however, two mechanisms for the transfer of energy from wind to waves have been identified and generally accepted. The first method, investigated by Phillips (1957) involves the resonant interaction of turbulent fluctuations in the air and the sea surface. The second method, investigated by Miles (1957-1962) involves energy transfer through shear between the air and the sea surface. These analytical descriptions of wave generation by wind are numerically demanding, and as a result the MIKE 21 numerical model uses a simplified, empirically derived formulation with source terms obtained from the Shore Protection Manual (1984).

As previously mentioned, the MIKE 21 numerical model accounts for energy losses due to wave breaking and bottom friction. Energy losses due to these phenomena have not yet been described analytically; however, many semi-analytical procedures to estimate these parameters have been proposed and shown to be reasonably accurate. MIKE 21 uses a model for energy loss and set-up due to the breaking of random waves proposed by Battjes and Janssen (1978); the description of bottom friction is based on the research of Svendsen and Jonsson (1980).

Wave Statistics from Wave Data

Although it is possible to obtain wave data through wave hindcasting, it is often desirable to obtain wave data directly. Wave data is useful for calibrating wave

hindcasting models, and can be used to predict extreme wave events if the recording period is sufficiently long. Direct wave data is particularly useful since nearshore effects such as refraction, shoaling and diffraction are included.

Frequently employed techniques for collecting wave data include recording the water surface elevation at a staff fixed to the seabed, recording the motions of a floating buoy, and recording pressure fluctuations in the water column. The net result of a wave data collection program is a set of traces of surface elevation with respect to time. From these traces, statistics such as the significant wave height and peak wave period are obtained to summarize the data.

Prior to the 1960's, wave traces were analyzed manually, and the significant wave height and peak period were estimated from characteristic quantities. During the early 1960's, random signal analysis techniques borrowed from the field of electrical engineering were applied to obtain statistics from wave traces. In particular, the Fast Fourier Transform algorithm developed by Cooley and Tukey (1965) allowed wave energy spectra to be obtained quickly and efficiently. The significant wave height and peak period are then obtained from the calculated wave spectra. Bendat and Piersol (1971) provide a detailed discussion of the Fast Fourier Transform algorithm and spectral analysis techniques.

1.2.3 HYDRODYNAMICS OF FLOATING STRUCTURES

The determination of wave forces on submerged and floating bodies has been the subject of extensive research within the field of naval architecture. A summary of this large area of study can be found in Newman (1977). Other important contributions in

this area include the work of Morison et al. (1950), who empirically derived an expression for the drag and inertia forces on a vertical cylinder, and MacCamy and Fuchs (1954), who used potential theory to solve the two-dimensional wave-structure interaction problem for a fixed vertical circular cylinder.

Floating bridges are often idealized as long horizontal cylinders with a rectangular cross-section. The hydrodynamic analysis of long horizontal cylinders has often been simplified by reducing the three-dimensional problem to a two-dimensional problem in the vertical plane. The two-dimensional results are then extended to three-dimensions by discretizing the bridge into elements and applying the two-dimensional results to the nodes after suitable modification to account for directional wave effects.

The two-dimensional diffraction problem for a horizontal cylinder was originally studied by Ursell (1949) for a circular section. Vugts (1968) conducted an experimental investigation of the hydrodynamic coefficients of cylinders with circular, triangular and rectangular cross-sections. The particular problem of oblique wave interaction with a cylinder of rectangular cross-section was studied by Garrison (1969), who used a Green's function procedure to solve the corresponding boundary value problem. Georgiadis and Hartz (1982) developed a boundary element program to obtain the hydrodynamic coefficients of a rectangular cylinder in water of arbitrary depth. More recently, Isaacson and Nwogu (1987) solved the diffraction problem of waves obliquely approaching a floating rectangular cylinder of finite length by means of a numerical procedure based on Green's theorem. The technique developed by Isaacson and Nwogu can be applied in deep and shallow water, and has been used in this thesis.

1.2.4 DIRECTIONAL WAVE EFFECTS ON FLOATING STRUCTURES

Directional wave effects on long floating structures have been quantified through explicit representation of the short-crested wave field and through superposition of infinite-crested waves with numerous frequencies and directions of propagation. Hutchison (1984) has shown that both techniques are logically consistent.

Hartz (1981) explicitly accounted for the short-crested behavior of a wave field by applying a frequency dependent reduction factor ("Spatial Correlation Factor") to the wave forces applied at the nodes of a time domain finite element analysis. The reduction factor was developed empirically through the analysis of field data. Some researchers have extended this technique by deriving coherency functions from the directional wave spectrum. These coherency functions describe the correlation of wave forces at different points along a structure. The coherency functions are used to generate covariance matrices for wave forces that are applied to frequency or time domain analyses. Langen and Sigbjornsson (1981), Hartz and Georgiadis (1982) and Hutchison (1984) have described this technique.

Methods that quantify directional wave effects by superposing force contributions from infinite crested waves with numerous frequencies and directions of propagation have been described by Engel and Nachlinger (1982) and Isaacson and Nwogu (1987). Both of these papers employ a frequency domain analysis. Isaacson et al. (1997) conducted a time domain analysis of a widened version of the Okanagan Lake Floating Bridge by superposing force contributions from infinite crested waves; the methodology described in this paper has been used in this thesis.

1.2.5 SLOWLY-VARYING WAVE DRIFT FORCES

Slowly-varying wave drift forces are a second order phenomenon, and are proportional to the square of the wave amplitude. Wave drift forces were originally studied for uni-directional monochromatic waves. Maruo (1960) showed that the wave drift force due to regular waves is steady, and can be derived from the first-order velocity potential. Further research in this area was conducted by Newman (1967), who derived a formulation for the wave drift moment, and Longuet-Higgins (1977), who derived a widely applied formulation for the steady wave drift force as a function of the reflection and transmission coefficients of a structure.

The wave drift force due to irregular waves varies slowly with time, and a rigorous solution of the problem requires computation of the second-order velocity potential. Wave drift forces in uni-directional irregular seas were originally studied by Newman (1974). Newman developed a technique for calculating wave drift force time series that approximates the wave spectrum as narrow banded. As a result of this approximation, the problem can be solved in terms of the first-order velocity potential, and the computational effort is greatly reduced. Marthinsen (1983) studied wave drift forces in directional irregular waves. He showed that Newman's index approximation can be applied to both the frequency and directional distribution of wave energy. Kim and Yue (1989) have also studied this topic, and their expression for slowly-varying wave drift force in directional seas has been applied in this thesis.

1.2.6 DYNAMIC ANALYSIS OF FLOATING STRUCTURES

The dynamic analysis of floating structures is a multi-disciplinary problem that involves both hydrodynamics and structural dynamics. The first step in the dynamic analysis of a floating structure is the determination of hydrodynamic coefficients and hydrostatic stiffnesses. Next, the structural stiffness, mass and damping matrices must be assembled. Finally, the equations of motion of the structure must be solved by an appropriate numerical method.

A literature review of the hydrodynamic analysis has already been presented in Section 1.2.3. The determination of hydrostatic stiffnesses of ships and floating structures has received much attention within the field of naval architecture, and the theory can be found in many texts, notably Goldberg (1988).

A general discussion of the mass, damping and stiffness matrices of floating and offshore structures can be found in Sarpkaya and Isaacson (1981). Depending on the characteristics of the structure, the structure may be modeled by the stiffness method or an approximate method such as the finite element method. Readers are referred to texts by Hibbler (1995) and Bathe (1996) for further information on these methods.

Once the mass, damping, and stiffness matrices of a structure have been assembled, a method must be chosen to solve the equations of motion. If the system is classically damped, a modal analysis can be used to uncouple the equations of motion, and these equations can be solved in closed form if the excitation is a simple function. If the system is non-classically damped, non-linear, or subject to complex excitation, the equations of motion must be solved numerically. Numerical techniques for solving linear systems include the central difference method and Newmark's method. The average

acceleration method and Wilson's method can be used to solve non-linear systems. Readers are referred to general texts on this subject by Humar (1990), Clough and Penzien (1993) and Chopra (1995).

1.3 SCOPE OF THE PRESENT WORK

The existing bridge across Okanagan Lake was designed by Swan Wooster and Partners of Vancouver, Canada in 1956. Wave loading was not considered in the design, and the bridge was constructed to resist only wind and ice loads. The bridge currently has three lanes for traffic, and one lane alters direction in rush hours to accommodate heavy traffic. Projected population growth in the region will make it necessary to widen the bridge to four lanes.

This thesis describes a dynamic analysis of a four-lane floating bridge which was designed by Westmar Consultants Inc. of North Vancouver, Canada as a proposed replacement for the existing bridge. The original intent of this thesis was to model the existing bridge, calibrate the wave hindcasting procedure with wind and wave data collected at the site, and calibrate the structural model with mooring cable tension data. Unfortunately, no major storm events occurred prior to the writing of this thesis and therefore calibration of the structural model with cable tension data was not possible. As a result, it was decided that a dynamic analysis of the proposed bridge would be more useful since the results of this analysis could be referenced during final design of the bridge.

A flow chart of the steps involved in the dynamic analysis is presented in Figure 3. The analysis includes the calculation of design wind velocities, wave hindcasting, a

hydrodynamic analysis and a time domain dynamic analysis using the finite element method. A computer program developed by the Danish Hydraulic Institute called MIKE 21 NSW (Nearshore Spectral Wave) was used for wave hindcasting. The wave hindcasting results were compared with field data collected at the bridge site. A program called HAFB (Hydrodynamic Analysis of a Floating Breakwater), written by Isaacson and Nwogu at the University of British Columbia was used for the hydrodynamic analysis. A program called FORCETIME, developed by the author was used to assemble the wave force time series. The dynamic analysis was performed using a commercial finite element program called COSMOS/M developed by the Structural Research and Analysis Corporation in the United States of America.

With the exception of FORCETIME, none of the above mentioned computer programs were developed as a result of this research. As a result, the primary contribution of this thesis is to apply state-of-the-art theories and techniques to the analysis of a long floating structure and indicate their potential application within an engineering context. The primary objective of the research was to obtain maximum values of the following parameters during a 100-year storm:

- sway, heave and roll displacements of the bridge;
- bending moments within the pontoons;
- mooring cable tensions.

In addition, the variability in maximum responses was evaluated by performing several simulations and calculating sample statistics. The influence of slowly-varying wave drift forces on the response of the bridge was also investigated by conducting a simulation with a static drift force.

2. DESCRIPTION OF THE BRIDGE AND FIELD DATA

2.1 BRIDGE LOCATION AND DIMENSIONS

The Okanagan Lake Floating Bridge is located in Kelowna, British Columbia, Canada. The bridge forms part of Highway 97, an important north-south link in central British Columbia. A map of the region is presented in Figure 4. The proposed four-lane bridge will be moored 25 m to the north of the existing bridge, which will be decommissioned after the new bridge is operational.

Okanagan Lake is approximately 340 m above sea level, and is situated in a valley between mountain ridges with heights reaching 1,500 m. The depth of water at the crossing for the proposed bridge varies from about 5 m at the east end of the floating section to 50 m at the center of the floating section.

The floating bridge is located at a bend in the lake. The section of the lake to the north of the bridge has a north-south orientation, with an average width of 4 km and a length of approximately 40 km. The section of the lake to the south of the bridge has a southwest-northeast orientation with a length of approximately 25 km and an average width of 5 km. The physical geography of the region surrounding the bridge site tends to funnel wind down the length of the lake.

The entire length of the proposed bridge is 1,075 m. Plan and elevation views of the bridge are shown in Figure 5. The proposed bridge consists of several sections:

- a 278 m long approach span, at the west end of the bridge;
- a 58 m long transition span between the west approach and the pontoon section;

- a 673 m long pontoon section, formed by 12 pontoon units rigidly connected together;
- a 65 m long east transition span between the pontoon section and the shore.

The west transition span is elevated 18 m above the lake surface to allow the passage of boats. The elevated transition span eliminates a lift span system on the existing bridge which periodically halts traffic flow.

The majority of the pontoons are 60.93 m long and 22.28 m wide. The draft of these pontoons varies from 4.3 m at the east end of the floating section to 2.5 m at the centre of the floating section. The pontoon at the west end of the floating section is 17.75 m long and 22.28 m wide, and has a maximum draft of 4.0 m. The increased draft of the pontoons at the ends of the floating section provides extra buoyancy to equilibrate the support reactions of the transition spans and elevated road deck. The pontoons will be constructed of reinforced concrete, and will be divided into cells and filled with styrofoam to minimize the likelihood of sinking.

The pontoon section is given lateral stability by 24 cables, with 12 cables on each side of the bridge. It is given longitudinal stability by the east transition span that connects the floating section to a concrete caisson on the shore. The mooring cables are generally equally spaced, and are connected to plow-like anchors embedded in the lake bottom. The cables are all pre-tensioned to approximately the same load level (500 kN when the lake is at mean water level) and all have the same cross-sectional area and modulus of elasticity. The cables in shallower water are stiffer since they are shorter.

2.2 FIELD DATA COLLECTION

A field data collection program at the existing bridge was commenced by Westmar Consultants Inc. in February 1998. The program includes the collection of wind data, pressure in the water column (to allow the computation of wave heights), and cable tensions. Wind data at the bridge and nearby airports is also available from the Atmospheric Environment Service of Canada (AES).

2.2.1 WIND DATA

There is no long-term record of wind velocity at the bridge site. As a result, it was necessary to correlate the wind velocities measured at the bridge site with long term records collected at Kelowna and Penticton airports. A description of the wind records from these sources follows.

Kelowna Airport

Kelowna airport is located 13 km to the north-east of the Okanagan Lake Floating Bridge at an elevation of 430 m. It is not situated on Okanagan Lake, and consequently the wind conditions at the airport may not be used directly for wave hindcasting. The wind data at the airport has been collected by the AES, and is available in hourly and Model B formats. The Model B format is a summary of wind speed and direction over the entire recording history. The wind speed is the 2-minute mean wind speed recorded on the hour; wind direction is recorded on an 8-point compass. The record duration is approximately 30 years, and therefore this wind data is statistically reliable for extreme wind speed computation.

Penticton Airport

The Penticton airport is located on Okanagan Lake 45 km to the south of the Okanagan Lake Floating Bridge (See Figure 4) at an elevation of 344 m. Although Penticton Airport is further away from the bridge site than the Kelowna airport, it is situated at the same elevation as the lake, and therefore the surrounding topography more closely resembles the bridge site. The wind data at the airport has been collected by the AES, and is available in hourly and Model B formats. The wind speed is the 2-minute mean wind speed recorded on the hour; wind direction is recorded on an 8-point compass. The record duration is approximately 45 years, and is the most statistically reliable source of wind data available for extreme wind speed computation.

Floating Bridge Site

Wind data has been collected at the bridge site for two periods. The first period was initiated by the AES and spans from June 1971 to August 1976. This data was collected by means of an anemometer attached to the top of the east span lift tower. The anemometer measured hourly average wind speed (km/hr) and wind direction on a 16-point compass.

The second period of wind data recording began on February 1998 and was initiated by Westmar Consultants Inc. This data is being collected by means of a RM Young 05103LK wind sensor mounted on top of a luminaire pole on the south sidewalk at the centre of the bridge. The wind sensor came pre-calibrated from the factory. Wind speed and direction are measured every five seconds, and at the end of each hour,

statistics are processed. The statistics include hourly average wind speeds, and 2-minute mean wind speeds measured on the hour.

2.2.2 PRESSURE DATA

One pressure transducer (Omega PX437-015GI) is mounted on both the north and the south anchor cables at the centre of the bridge. The north transducer is installed at a depth of approximately 4.1m, and the south transducer is installed at a depth of about 3.7m. The total water depth at the transducer locations is approximately 50 m. The pressure transducers came with calibration curves from the factory. This calibration was checked by placing the transducers in various depths of water and checking the output signal. In addition, the transducers were placed in a wave flume at UBC's hydraulics laboratory, and the output was recorded to ensure the transducers could respond to rapidly varying dynamic wave pressure.

Pressure data is continuously collected at a rate of 2 Hz, and is compiled into a mean and standard deviation every half-hour and recorded in a data file. Pressure data is also recorded when the 2-minute average wind speed exceeds a threshold value (25 km/hr). When the threshold wind speed is exceeded, the pressure data is recorded for 5 minutes at 0.5 second intervals and then data files are recorded two more times at 15 minute intervals. If the 2-minute wind speed exceeds the threshold value 45 minutes after the original threshold exceedance, the process repeats.

3. DESIGN WAVE DETERMINATION METHODOLOGY

3.1 DETERMINATION OF THE DESIGN WIND VELOCITIES

As discussed in Chapter 2, wind data is available at the bridge site for a total of approximately 5 years. The short duration of this record makes it inadequate for calculating large return period wind speeds. As a consequence, longer wind records available at Kelowna and Penticton airports were used to determine the design 100-year return period wind velocities.

The 100 year winds at Kelowna and Penticton airports corresponding to various directions and durations were determined by fitting a Type I asymptotic (Gumbel) distribution to AES Model B wind data. The equation for the Gumbel distribution is as follows:

$$\alpha(V-\beta) = -\ln[-\ln(P(V))] \tag{3.1}$$

where V is the wind speed, $P(V)$ is the cumulative probability of the wind speed and α and β are scale parameters determined through linear regression. The exceedance probability, $1\text{-}P(V)$ is equal to the recording interval divided by the return period.

Once the design wind speeds at both airports were calculated, they were multiplied by scaling factors to produce the design wind velocities at the bridge site. The scaling factors were determined from the slope of a best-fit line fitted to scatter plots of hourly wind data recorded at the bridge and airports over the period from June 1971 to August 1976.

3.2 HINDCASTING THE DIRECTIONAL WAVE SPECTRUM

3.2.1 DIRECTIONAL WAVE SPECTRA AND SPECTRAL ANALYSIS

Basic linear wave theory predicts a sinusoidal water surface elevation. In nature, water surfaces are random and irregular, and the long-crested sinusoidal waves described by linear wave theory do not exist. The dynamic response of structures depends critically on the frequency of the excitation. As a result, it is necessary to quantitatively describe the random water surfaces that occur in nature. Coastal engineers use the theory of random signal analysis to accomplish this.

Several fundamental assumptions are made in the mathematical description of an irregular water surface through random signal analysis. The first assumption is that the water surface elevation is stationary, homogeneous and ergodic. This means that the statistical properties of the water surface do not change in either time or space, and that a single measured realization of the water surface elevation is typical of any measured realization.

The second assumption is that the random water surface elevation can be adequately described by superposing numerous linear waves with different frequencies, phases and directions of propagation. These assumptions allow one to describe the random water surface by means of Fourier series and power spectra. A brief review of Fourier series and power spectra is presented in the following paragraphs.

Review of Fourier Series and Power Spectra

Assume that $x(t)$ is a measured realization of water surface elevation measured at N equally spaced points in time Δt apart in the range $(0,T)$. The data values at each time step are:

$$x_n = x(n\Delta t) \quad \text{for } n = 0, 1, 2, \ldots, N\text{-}1 \tag{3.2}$$

The wave elevation record $x(t)$ can be represented by superposing numerous sinusoidal waves with different frequencies and amplitudes in a Fourier series (in complex notation):

$$x(t) = \sum_{n=-\infty}^{\infty} X_n e^{-i2\pi f_n t} \tag{3.3}$$

In this equation, X_n are the amplitudes and f_n are the frequencies of each Fourier component. The amplitudes of the Fourier components are determined from the Fourier transform of the record:

$$X(f_n) = \int_0^T x(t) e^{-i2\pi f_n t}\, dt \tag{3.4}$$

However, since $x(t)$ is sampled at discrete intervals, the Fourier components must be calculated at discrete frequencies. These frequencies are normally chosen at equal intervals defined by:

$$f_k = \frac{k}{T} = \frac{k}{N\Delta t} \quad \text{for } k = 0, 1, 2, \ldots, N\text{-}1 \tag{3.5}$$

At these frequencies, the discrete version of equation (3.4) is as follows:

$$X(f_k) = \Delta t \sum_{n=0}^{N-1} x_n \exp\left[-i\frac{2\pi kn}{N}\right] \quad \text{for } k = 0, 1, 2, \ldots, N\text{-}1 \tag{3.6}$$

The Fourier components, $X(f_k)$ are normally calculated by means of the highly efficient Fast Fourier Transform (FFT) algorithm.

The Fourier components can be used to create a power spectrum of the sea state. The power spectrum gives the relationship between wave frequency and spectral density, $S(f_k)$. The one-sided power spectrum is given by the following equation:

$$S(f_k) = \frac{2}{N\Delta t}\left|X(f_k)\right|^2 \quad \text{for } k = 0, 1, \ldots, N/2 \tag{3.7}$$

A brief inspection of equation (3.7) reveals that spectral density is proportional to wave amplitude squared. The spectral density is therefore a measure of the energy present in the waves at that frequency. For this reason, power spectra of wave records are often called energy spectra. Typical wave energy spectra have low energy at low and high frequencies, and reach a maximum value at an intermediate frequency, known as the peak frequency.

Directional Wave Energy Spectra

Numerous researchers have measured sea states, and have proposed empirical formulae for wave energy spectra. Bretschneider (1961) proposed one of the most commonly used energy spectra. The Bretschneider spectrum is defined by the peak frequency, f_p and significant wave height, H_s of the sea state and is given by the formula:

$$S(f) = \frac{5H_s^2}{16 f_p}\left(\frac{f}{f_p}\right)^{-5} \exp\left[-\frac{5}{4}\left(\frac{f}{f_p}\right)^{-4}\right] \tag{3.8}$$

The significant wave height is the average height of the highest 33% of the waves in a wave train. The Joint North Sea Wave Project (JONSWAP) spectrum is a modified version of the Bretschneider spectrum, and has a larger concentration of wave energy

about the peak frequency. An example of a JONSWAP spectrum is presented in Figure 6. The JONSWAP spectrum is based on extensive observations taken in fetch limited conditions in the North Sea and has been used in this thesis. The JONSWAP spectrum is given by the formula:

$$S(f) = \alpha H_s^2 f_p^4 f^{-5} \exp\left[-1.25\left(\frac{f}{f_p}\right)^{-4}\right]\gamma^{\exp\left[-\left(\frac{f}{f_p}-1\right)^2/2\sigma^2\right]} \tag{3.9}$$

$$\alpha = \frac{0.0624}{0.230 + 0.0336\gamma - 0.185(1.9+\gamma)^{-1}}$$

$$\sigma = \begin{Bmatrix} \sigma_a : f \le f_p \\ \sigma_b : f > f_p \end{Bmatrix}$$

with $\sigma_a = 0.07$

$\sigma_b = 0.09$

$\gamma = 3.3$

The spectra discussed above describe only the distribution of wave energy with frequency. When determining the response of long floating structures to waves, directional wave effects, or wave short-crestedness must also be considered. The directional wave spectrum, $S(f,\theta)$ describes the relationship between wave energy and wave frequency and direction. An example of a directional wave spectrum is shown in Figure 7.

Directional wave spectra are often expressed as the product of a one-dimensional spectrum and a directional spreading function:

$$S(f,\theta) = S(f)G(f,\theta) \tag{3.10}$$

where $G(f,\theta)$ is the directional spreading function. Further simplification is achieved by assuming that wave direction is independent of frequency and therefore $G(f,\theta)$ becomes $G(\theta)$. The directional spreading function has the property:

$$\int_{-\pi}^{\pi} G(\theta)d\theta = 1 \tag{3.11}$$

As a result, the directional spreading function does not amplify the total energy present in the one-dimensional spectrum.

Numerous directional spreading function formulations have been proposed. One of the most commonly used directional spreading functions is the cosine power function proposed by Longuet-Higgins et al. (1961). The cosine power formulation is as follows:

$$G(\theta) = C(s)\cos^{2s}(\theta) \tag{3.12}$$

where θ is measured from the mean direction of wave propagation and the directional spreading index, *s* controls the dispersion of wave energy in the θ direction. As the directional spreading index becomes larger, the waves approach uni-directionality. The normalizing coefficient *C(s)* is chosen such that equation (3.11) is satisfied.

Borgman (1969) proposed an alternative formulation for the cosine power directional spreading function:

$$G(\theta) = \begin{cases} C'(s)\cos^{2s}(\theta) & \text{for } |\theta| < \pi/2 \\ 0 & \text{otherwise} \end{cases} \tag{3.13}$$

where θ is measured from the mean direction of wave propagation and the directional spreading index, *s* controls the dispersion of wave energy in the θ direction. Again, the normalizing coefficient *C'(s)* is chosen such that equation (3.11) is satisfied. This formulation of the cosine power directional spreading function is shown in Figure 8 for various values of the directional spreading index.

The spreading function formulations discussed above are an approximation to those observed in nature. The appeal of the cosine power formulations rests largely with their simplicity. Numerical wave hindcasting programs such as MIKE 21 can calculate direction spreading functions of arbitrary form based on the wind field and bathymetry in the area of interest.

3.2.2 DIRECTIONAL WAVE HINDCASTING

As previously mentioned, the MIKE 21 NSW computer program has been used for wave hindcasting in this thesis. MIKE 21 is a stationary numerical model that determines the directional wave spectrum from the wind field at a series of grid locations based on a numerical integration of the wave action balance equation. The model accounts for wave generation by wind, energy losses due to wave breaking and bottom dissipation, refraction, and wave-current interaction.

The program uses an Eulerian approach, and solves the directional action balance equation on a rectangular grid in x,y,θ space. The wave action balance equation generally states that the rate of change of wave energy at a location equals the energy being convected to and from the location plus the local transfer of energy between the wind field and the waves.

Wave energy is represented in the frequency domain by the two-dimensional wave action spectrum, $A(\omega,\theta;x,y,t)$. The wave action spectrum is related to the wave energy spectrum by the following equation:

$$A(\omega,\theta;x,y,t) = S(\omega,\theta;x,y,t)/\sigma \tag{3.14}$$

where $A(\omega,\theta;x,y,t)$ and $S(\omega,\theta;x,y,t)$ are the directional wave action and energy spectra respectively and the relative frequency, σ is defined as:

$$\sigma = \omega - \underline{k} \cdot \underline{V} \tag{3.15}$$

In this equation, $\underline{k}$ is the wave number vector, $\omega = 2\pi f$ is the angular frequency and $\underline{V}$ is the current velocity vector. The action balance equation is used as opposed to the more common energy balance equation to account for the possible presence of currents. The complete action balance equation can be written as follows:

$$\frac{\partial A}{\partial t} + \frac{\partial}{\partial \omega}(c_\omega A) + \frac{\partial}{\partial x}(c_x A) + \frac{\partial}{\partial y}(c_y A) + \frac{\partial}{\partial \theta}(c_\theta A) = E \tag{3.16}$$

where E is the energy source term and c_x, c_y and c_θ are the energy propagation speeds in the x,y and θ directions. The propagation speeds are components of the group velocity $\underline{c}$, given by linear wave theory as:

$$\underline{c} = \frac{\partial \omega}{\partial k} \frac{\underline{k}}{k} \tag{3.17}$$

Solving the complete version of the action balance equation requires considerable computational effort. As a result, the complexity of the problem has been reduced by making several simplifications. The first simplification is achieved by making the model stationary (independent of time). As a result, the first and second terms in equation (3.16) become zero, and the model produces only fetch-limited solutions.

The complexity of the problem is further reduced by parameterizing the action balance equation in terms of the zero-th and first moments of the action spectrum. The n^{th} moment of the action spectrum is defined as follows:

$$m_n(\theta) = \int_0^\infty \omega^n A(\omega,\theta) d\omega \tag{3.18}$$

For the purposes of calculating the spectral moments, the action spectrum is assumed to be derived from a standard JONSWAP energy spectrum. Further simplification is obtained by taking the group velocity (and therefore the propagation speeds) equal to their corresponding speeds at the mean frequency, ω_o. The group velocity is therefore written:

$$\underline{c_o} = \frac{\partial \omega_o}{\partial k_o} \frac{\underline{k_o}}{k_o} \tag{3.19}$$

The equations resulting from the parametrization and the above mentioned simplifications are as follows:

$$\frac{\partial}{\partial x}(c^*_{ox} m_o) + \frac{\partial}{\partial y}(c^*_{oy} m_o) + \frac{\partial}{\partial \theta}(c^*_{o\theta} m_o) = E_o \tag{3.20}$$

$$\frac{\partial}{\partial x}(c^{**}_{ox} m_1) + \frac{\partial}{\partial y}(c^{**}_{oy} m_1) + \frac{\partial}{\partial \theta}(c^{**}_{o\theta} m_1) = E_1 \tag{3.21}$$

where c^*_{ox}, c^*_{oy} and $c^*_{o\theta}$ in equation (3.20) and c^{**}_{ox}, c^{**}_{oy} and $c^{**}_{o\theta}$ in equation (3.21) are the energy propagation speeds through x,y,θ space of m_0 and m_1 respectively. E_0 and E_1 are the parameterized source functions for m_0 and m_1 respectively.

As previously mentioned, the MIKE 21 computer program accounts for energy losses due to wave breaking and bottom friction. The program uses a model for energy

loss and set-up due to the breaking of random waves proposed by Battjes and Janssen (1978). The description of bottom friction is based on the research of Svendsen and Jonsson (1980). Readers are referred to these sources for further information.

The partial differential equations (3.20) and (3.21) are solved numerically. A finite-difference technique is applied for discretization of the differential equation in x,y,θ space. Rectangular grid spacing is used, and the system of equations is solved using a once-through marching procedure in the x-direction. The output of MIKE 21 includes the significant wave height, mean spectral period, mean wave direction and directional standard deviation of the directional spreading function at each grid point in the model domain. The directional standard deviation can be related to the spreading index, s in the cosine squared directional spreading function formulation.

Design wave conditions were calculated for north and south storms with a return period of 100 years. This was accomplished by applying the design wind velocities to MIKE 21 models of the north and south sections of Okanagan Lake. The digitized bathymetries of the north and south fetches are shown in Figures 9 and 10. Results from the MIKE 21 model of the southern portion of the lake were compared with field data.

3.3 CALIBRATION OF THE HINDCAST SEA STATE WITH FIELD DATA

When modeling complex phenomena such as wave generation by wind, it is desirable to compare the model results with field data. As discussed in Section 2.2, a field data collection program is in place at the bridge site. The wind velocities and wave statistics collected in this program have been compared with output from the MIKE 21

wave hindcasting computer program. At the time of writing, field data was available for approximately one year, and several minor storm events were recorded.

Wave statistics were recorded by means of two pressure transducers, one mounted on the north and south anchor cables at the centre of the bridge. The records of pressure as a function of time were converted to pressure spectra by means of the Fast Fourier Transform algorithm described in Section 3.2.1. A cosine squared (Hanning) filter was first applied to the time-series data to reduce side lobe leakage and thereby increase the accuracy of the spectral estimate. The pressure spectra were converted to wave energy spectra by means of a linear transfer function:

$$S_n(f) = (H_{pn}(f))^2 S_p(f) \tag{3.22}$$

where $H_{pn}(f)$ is the linear transfer function and $S_p(f)$ and $S_n(f)$ are the pressure and wave energy spectra respectively. The transfer function for conversion from pressure spectra to wave energy spectra (assuming deep water) is as follows:

$$H_{pn}(f) = e^{-kz} \tag{3.23}$$

where k is the wave number and z is the depth of the pressure transducer below the still water level.

The pressure transducers are located approximately 20 m from the pontoon walls. As a result, the pressure records include both incident and reflected waves. The incident and reflected wave spectra were separated by means of a linear transfer function:

$$S_{n_i}(f) = (K_r)^2 S_n(f) \tag{3.24}$$

The reflection coefficient of the bridge, K_r at each frequency was calculated using diffraction theory. The resulting incident wave energy spectra were smoothed over

frequency to reduce the standard error of the spectral estimate. The significant wave height and peak period of the spectra were then calculated.

The sensitivity of the pressure transducers prevents them from measuring waves with a period less then 2.5 s. This restriction greatly limits the number of measured wave energy spectra available for comparison. In fact, examination of the field data reveals that only 14 recorded wave spectra are suitable for comparison. The maximum hourly average wind velocity recorded in these storms is 40 km/hr.

The MIKE 21 wave hindcasting program was run for the wind speed and directions recorded during each of the 14 storm events. The significant wave height and peak period calculated by MIKE 21 were compared to the measured values, and the results are presented in Table 1. Energy dissipation due to bottom friction and wave breaking were not included in the MIKE 21 simulations, and therefore upper bound solutions for wave height and period were obtained.

The predicted and measured significant wave heights differ by a maximum of 31% and a minimum of –11%, with an average difference of 9 %. The predicted and measured peak wave periods differ by a maximum of –6 % and a minimum of –25%, with an average difference of -17%. This comparison suggests that MIKE 21 provides on average, a small overestimate of the significant wave height, but consistently underestimates the peak period of the waves. The wave height results suggest that energy-dissipating phenomena such as bottom friction and wave breaking should be included in the model, however the wave period results suggest an opposite approach.

Some error can be expected in the measured wave parameters since long-term statistics are being estimated by a relatively short sample. This source of error is

common to most spectral analyses. However, the difference in measured and calculated wave parameters can also be attributed to other sources of error including the following:

- inaccuracy in the calculated reflection coefficients of the bridge;
- the presence of radiated waves due to bridge motion;
- the motion of the mooring cables to which the pressure transducers have been attached;
- inaccuracy in the measured wind speed due to boundary layer effects;
- variability in the wind velocity over the lake due to topography and the finite size of the weather systems.

Despite these numerous sources of error, the MIKE 21 program provides on average, a reasonable estimate of the wave conditions. As a result, increased confidence has been ascribed to the wave hindcasting results for the 100-year storm, but detailed calibration with the limited field data available has not been performed.

4. WAVE LOAD DETERMINATION

4.1 DEVELOPMENT OF THE RANDOM, MULTI-DIRECTIONAL SEA

The random, multi-directional wave field at the bridge is completely defined by the directional wave spectrum. This directional wave spectrum can be used to create a synthetic record of wave elevation as a function of time at any point along the bridge. The wave elevation record can in turn be combined with the force coefficients and phases determined in the hydrodynamic analysis to produce a record of force as a function of time at any point along the bridge for any degree of freedom.

For a single wave train, the water surface elevation η as a function of time t and distance x in the direction of wave travel is given by linear wave theory as:

$$\eta(x,t) = a\cos(kx + \omega t - \phi) \tag{4.1}$$

where a, k, ω, ϕ are the wave amplitude, wave number, angular frequency and phase of the wave train. The wave number is related to the angular frequency at a water depth d through the linear dispersion relation:

$$\frac{\omega^2}{k} = g\tanh(kd) \tag{4.2}$$

where g is the acceleration due to gravity. This expression must be solved iteratively since k appears on both sides of the equation.

A random, unidirectional wave field can be obtained by superposing waves with numerous amplitudes, frequencies and phases; this wave field is given by the expression:

$$\eta(x,t) = \sum_{i=1}^{n} a_i \cos(k_i x + \omega_i t - \phi_i) \tag{4.3}$$

where a_i, k_i, ω_i, ϕ_i are the wave amplitude, wave number, angular frequency and phase of each component of the wave train and the index i refers to each wave frequency.

When creating a synthetic random wave record that conforms to a particular wave spectrum, the spectrum is discretized into a number of frequency intervals, Δf_i. The wave amplitude at each interval is given by the equation:

$$a_i = \sqrt{2S(f_i)\Delta f_i} \tag{4.4}$$

The phase of the wave train at each frequency is usually assumed to be a random number uniformly distributed between 0 and 2π.

Equation (4.3) describes waves with an infinite crest length. As previously mentioned, this model is inappropriate when determining the forces on long structures, and consequently, wave short-crestedness must be taken into account. A random, multi-directional wave record can be created by superposing waves with numerous frequencies and directions of propagation. The water surface elevation at any point x, y on a horizontal plane and at any time instant t is given by the expression:

$$\eta(x,y,t) = \sum_{i=1}^{n}\sum_{j=1}^{m} a_{ij}\cos(k_i x\cos\theta_j + k_i y\sin\theta_j + \omega_i t - \phi_{ij}) \tag{4.5}$$

where θ is the direction of wave propagation, the subscript j corresponds to each wave direction and the subscript i corresponds to each wave frequency. A three-dimensional water surface elevation profile generated by this equation is shown in Figure 11.

When creating a synthetic random wave record that conforms to a particular wave spectrum, the spectrum is discretized into a number of frequency intervals, Δf_i and wave

directions $\Delta\theta_j$. This procedure yields n_f x n_d regular wave components. The wave amplitude at each frequency and direction is given by the equation:

$$a_{ij} = \sqrt{2S(f_i, \theta_j)\Delta f_i \Delta\theta_j} \tag{4.6}$$

The phase of the wave train at each frequency and direction is usually assumed to be a random number uniformly distributed between 0 and 2π.

Two methods are commonly used to discretize the wave spectrum in frequency: the equal frequency method and the equal energy method. A complete review of both of these techniques is provided in Goda (1985). In the equal frequency method, the spectrum is divided such that each frequency interval, Δf_i is equal. In the equal energy method, the spectrum is discretized such that each frequency interval contains the same amount of energy. In both methods, the frequency corresponding to each interval is selected as the average of the interval's lower and upper bounds.

The equal energy method was used in this thesis and is preferable because the regular wave components at each frequency are less likely to form harmonics. As a result, the repetition time of a wave record synthesized by the equal energy method is larger. Angle intervals are usually specified as constant since there is no danger of harmonic formation.

4.2 DEVELOPMENT OF THE FORCE TIME SERIES

The force time series are created by combining each regular wave component in the random, multi-directional sea with appropriate hydrodynamic coefficients. The force exerted by a regular wave component on a structure segment of length Δ can be written:

$$F(x,t) = aCR\Delta\cos(kx\cos\theta + \omega t - \phi - \varepsilon) \tag{4.7}$$

where ε is the phase difference between the wave elevation and the force and C is the force or moment per unit wave amplitude:

$$C = \frac{F}{0.5H} = \frac{C_f(\omega,\theta)0.5\rho gHb}{0.5H} = C_f(\omega,\theta)\rho gb \tag{4.8}$$

The force coefficient $C_f(\omega,\theta)$ is obtained from the hydrodynamic analysis as described in Section 4.3. This coefficient varies with frequency and wave direction and is calculated for each degree of freedom (sway, heave and roll). In the above expression, F is the total force on the structure segment, H is the wave height, ρ is the density of water and b is a characteristic dimension of the structure. The structure is assumed to lie on the x-axis (y=0) and the angle θ is measured counterclockwise from the positive x-axis.

The variable R in equation (4.7) is a reduction factor that quantifies the reduction in wave force due to oblique wave approach. This reduction factor is obtained by calculating the force caused by a wave approaching a structure segment at an oblique angle and then finding the maximum value of the force over one wave period. This result is then non-dimensionalized by dividing by the force caused by a wave approaching the structure normally. The reduction factor is a function of wavelength, wave direction and structure segment length, and is given by the expression:

$$R = \frac{\sin(k\Delta/2\cos\theta)}{k\Delta/2\cos\theta} \tag{4.9}$$

This reduction factor is plotted as a function of $k\Delta$ for various values of incident wave angle, θ in Figure 12.

The total force on a structure segment of length Δ_k in degree of freedom q is obtained by summing the contributions from regular wave components in frequency and direction:

$$F_{kq}(t) = \Delta_k \sum_{i=1}^{n} \sum_{j=1}^{m} a_{ij} C_{ijq} R_{kij} \cos(k_i x \cos\theta_j + \omega_i t - \phi_{ij} - \varepsilon_{ijq}) \tag{4.10}$$

The force time series for each structure segment and degree of freedom were calculated by means of a computer program called FORCETIME, which was developed by the author. FORCETIME takes the dimensional spectrum, number of frequencies, number of directions, mean wave direction and directional spreading index as input parameters. The desired record length, time-step, bridge model geometry and water depth at each node are also input parameters. The program performs a bi-linear interpolation on the output of the hydrodynamic analysis program to obtain the force coefficients and phases for each wave frequency, direction and degree of freedom.

4.3 HYDRODYNAMIC ANALYSIS

A wave diffraction program written by Isaacson and Nwogu (1987) called HAFB (Hydrodynamic Analysis of a Floating Breakwater) was used to obtain the hydrodynamic coefficients. The hydrodynamic coefficients include the force coefficients and phases used to create the force time series and the added masses and damping coefficients that are components of the finite element model of the bridge.

In general, rigid floating bodies can have motions with six degrees of freedom. These degrees of freedom correspond to three translational motions (surge, sway and heave) and three rotational motions (yaw, pitch and roll). The Okanagan Lake Floating Bridge has been idealized as an infinite semi-immersed horizontal cylinder with a rectangular cross-section. Motions in the surge, pitch and yaw degrees of freedom are small, and are therefore neglected.

Numerous simplifying assumptions are made during the hydrodynamic analysis. Firstly, flow separation is neglected, and the effects of viscosity are assumed to be confined to a thin boundary layer on the body surface. Furthermore, the fluid is assumed to be incompressible, and the flow irrotational. As a result of these assumptions, potential theory can be used to describe the motion of the bridge. Further simplification is achieved by assuming the cylinder is flexible, and the deflection of the cylinder is periodic along its length. As a result, the three-dimensional problem can be reduced to two-dimensions.

If the incident wave height and the oscillatory motions of the bridge are small, the problem is linear, and superposition can be used to separate the wave-structure interaction problem into two parts:

- wave diffraction due to waves incident on a fixed infinite cylinder;
- an infinite cylinder oscillating in sway, heave and roll generating waves in otherwise still water.

The first problem is commonly called the wave diffraction problem, and the solution of this problem provides the diffraction potential. The second problem is called the forced

motion problem; solution of this problem provides the forced motion potentials for sway, heave and roll.

The boundary value problems for the diffraction potential and the forced motion potentials are solved by a boundary integral method based on Green's identity. Green's identity relates the values of the potentials within the fluid region to the values of the potentials on the boundary and their normal derivative. The boundary is defined by the immersed body surface, the mean position of the free surface, the radiation surfaces and the seabed.

Once the velocity potentials have been determined, the exciting forces, phases, added masses and damping coefficients can be calculated. The dimensionless exciting force coefficients and phases can be obtained from the incident and diffracted potentials. The non-dimensional added mass and damping coefficients in sway, heave and roll are obtained from the forced motion potentials. The HAFB program also calculates reflection, transmission and wave drift coefficients by evaluating the asymptotic wave amplitude of the scattered waves at the appropriate radiation surfaces.

In order to calculate the hydrodynamic properties needed for the dynamic analysis, HAFB was run repeatedly with different frequency and direction waves. The force coefficients, phases and wave drift coefficients were then obtained at each frequency and direction. These coefficients and phases were then used as input for FORCETIME, the program that assembles the wave force time series and the slowly-varying wave drift force time series. The added mass and hydrodynamic damping coefficients were included in the structural model of the bridge, and were calculated only at the peak frequency of the incident wave spectrum.

4.4 SLOWLY-VARYING WAVE DRIFT FORCES

In Section 4.2, wave force time series were derived by superposing force contributions from numerous linear waves. This force acts at a frequency approximately equal to the peak frequency of the incident wave spectrum. Field observations have shown that wave induced forces can also occur at frequencies much lower and higher than the peak frequency of the incident wave spectrum. These forces are non-linear, and are termed difference and sum-frequency excitations. Difference-frequency excitations are also called wave drift forces, and are of particular importance because they can excite a low frequency resonance in a floating structure's mooring system.

Drift forces were originally studied for uni-directional, regular waves. In this situation, the waves have a single frequency, and the drift force is steady and independent of time. Researchers such as Maruo (1960), Newman (1967) and Longuet-Higgins (1977) showed that the steady wave drift force can be derived in terms of the first order velocity potential. Longuet-Higgins derived the following formula for the steady wave drift force for normally incident waves on an infinitely long horizontal cylinder:

$$F_D = \frac{1}{8}\rho g\left[1+\frac{2kd}{\sinh(2kd)}\right](1+K_r^{\,2}-K_t^{\,2})H_i^{\,2} \tag{4.11}$$

In this equation, K_r and K_t are the reflection and transmission coefficients discussed in Section 4.3 of this paper, and H_i is the incident wave height. Note that this force is quadratic with respect to wave height.

The total second order force caused by uni-directional irregular waves can be written as the sum of two terms, $F_1(t)$ and $F_2(t)$, the first and second order wave forces respectively:

$$F_1(t)+F_2(t)=\mathrm{Re}\sum_i a_i C_i e^{i\omega_i t}+\mathrm{Re}\sum_i\sum_j a_i a_j S_{ij} e^{i(\omega_i+\omega_j)t}+\mathrm{Re}\sum_i\sum_j a_i a_j * D_{ij} e^{i(\omega_i-\omega_j)t} \tag{4.12}$$

In this equation, a_i and a_j are the wave amplitudes and * denotes the complex conjugate of a quantity.

The first term in equation (4.12) is the first order force discussed in Section 4.2 and C_i is the force coefficient discussed in Section 4.3. This force coefficient is the linear transfer function between wave amplitude and force. The second term in equation (4.12) is the second order sum-frequency force, and S_{ij} is a quadratic transfer function which is the sum-frequency force caused by two unit amplitude waves with frequencies ω_i and ω_j. The third term in this equation is of more interest, and is the difference-frequency force or slowly-varying wave drift force. The term D_{ij} is the difference-frequency quadratic transfer function which is the drift force caused by two waves with unit-amplitude and frequencies ω_i and ω_j.

The quadratic transfer functions, S_{ij} and D_{ij} can be obtained only from a second order solution of the velocity potential. Solution of the second order potential problem is laborious and generally impractical in an engineering context. However, Newman (1974) developed a useful approximation that allows slowly-varying wave drift force time series to be calculated in terms of the first order velocity potential. If the wave energy spectrum is assumed to be narrow-banded, then the difference between the frequencies ω_i and ω_j will be small. As a consequence, the quadratic transfer function of the off-diagonal elements, D_{ij} can be approximated by the values on the diagonal D_{ii}, which do not depend on the second order problem. The transfer function D_{ii}, can be interpreted physically as

the second order steady force acting on a structure in regular waves of unit-amplitude and frequency ω_i and is derived in a manner analogous to equation (4.11). The expression for the slowly-varying wave drift force becomes:

$$F(t) \cong \mathrm{Re} \sum_i \sum_j a_i a_j * D_{ii} e^{i(\omega_i - \omega_j)t} \tag{4.13}$$

Newman states that the quantitative accuracy of the approximation may vary from one case to another, and cannot be rigorously established without some knowledge of the off-diagonal second order forces. However, Newman qualifies this statement by recognizing that knowledge of the off-diagonal elements is lacking in many situations of engineering interest, and therefore the index approximation approach offers the only possibility for quantifying slowly-varying wave drift forces.

The expression for the slowly-varying wave drift force in directional irregular seas can be written as follows:

$$F(t) \cong \mathrm{Re} \sum_i \sum_j \sum_k \sum_l a_{ik} a_{jl} * D_{ijkl} e^{i(\omega_i - \omega_j)t} \tag{4.14}$$

where the subscripts i and j refer to summation over frequency and the subscripts k and l refer to summation over direction. The term D_{ijkl} is the difference-frequency quadratic transfer function which is the drift force caused by two waves with unit-amplitude and frequencies ω_i and ω_j and directions θ_k and θ_l. Marthinsen (1983) has shown that Newman's index approximation can be applied to both the wave energy spectrum and the directional spreading function. As a result, the quadratic transfer function, D_{ijkl} can be simplified to D_{iikk}. A slowly-varying wave drift force time series for random, directional waves can therefore be written as:

$$F(t) \cong \mathrm{Re} \sum_i \sum_j \sum_k \sum_l a_{ik} a_{jl} * D_{iikk} e^{i(\omega_i - \omega_j)t} \tag{4.15}$$

The wave drift force coefficients, D_{iikk}, were obtained for each frequency and direction from the computer program HAFB described in Section 4.3. The slowly-varying force time series were then calculated by the program FORCETIME, and were applied only in the sway degree of freedom.

4.5 STRUCTURAL ANALYSIS

The final step in the dynamic analysis is to apply the wave force time series to a structural model of the bridge and determine its response. The equation of motion of the bridge is:

$$\mathbf{m\ddot{u} + c\dot{u} + ku = F(t)} \tag{4.16}$$

where **m** is the mass matrix, **c** is the damping matrix, **k** is the stiffness matrix and **u** is the displacement vector. The dot and double-dot superscripts represent first and second derivatives with respect to time.

The mass matrix, **m** includes both the mass of the bridge and the hydrodynamic added mass. Likewise, the damping matrix, **c** includes both structural and hydrodynamic damping. The stiffness matrix, **k** includes both the structural stiffness and the hydrostatic stiffness. The forcing function vector, **F(t)** is composed of the wave force time histories for each node and degree of freedom. In addition, a steady force due to wind is included at the appropriate nodes.

The bridge was modeled using a commercial finite element program called COSMOS/M. The program can accept up to 100 different force time series as input, and each force time history can have a maximum of 5,000 time steps.

Isometric and cross-sectional views of the finite element model of the Okanagan Lake Bridge are shown in Figures 13 and 14. The pontoon string is parallel to the x-axis, and the y-axis is oriented vertically. The model has a total of 660 degrees of freedom.

The pontoon string is modeled as a 3-dimensional "spine" beam located at the vertical and horizontal centre of gravity of the pontoons. The spine beam is divided into 24 three-dimensional beam elements, and nodes are placed at anchor cable locations and midpoints. The typical length of the beam elements is 30.48 m. Rigid beams link the spine beam to the following locations:

- the centre of buoyancy of each pontoon element;
- the centre of gravity of the elevated roadway deck;
- the points of attachment of the anchor cables;
- the still water level.

In addition, rigid beam elements located at each end of the floating section link the spine beam to the centre of gravity of the transition spans.

The mass, and mass moment of inertia of each pontoon section are applied to the corresponding 3-dimensional beam element. The elevated roadway and transition spans are modeled as point masses with appropriate masses and mass moments of inertia. The hydrodynamic added mass and damping are modeled as point masses and concentrated dampers located at the still water level. The added mass and damping are approximated

as constant, and equal to their respective values at the peak frequency of the wave energy spectrum.

The hydrostatic heave stiffness of the bridge is modeled by translational springs at the centre of buoyancy of each of the pontoon segments. The equation for the heave buoyancy stiffness of a pontoon segment of length Δ is as follows:

$$k_{heave} = \rho g B \Delta \tag{4.17}$$

where B is the beam of the pontoon segment. The hydrostatic roll stiffness is modeled by rotational springs at the centre of buoyancy of each of the pontoon segments. The equation for the roll buoyancy stiffness of a pontoon segment of length Δ is as follows:

$$k_{roll} = \rho g A[(S / A) + z_B - z_G]\Delta \tag{4.18}$$

where A is the volume of water displaced by the pontoon per unit length, z_B is the vertical coordinate of the centre of buoyancy and z_G is the vertical coordinate of the centre of gravity. The moment of inertia of the submerged cross-section of the pontoon, S is given (for a rectangular section) by:

$$S = \int_B x^2 dx = \frac{B^3}{12} \tag{4.19}$$

When a floating body rolls, the centre of buoyancy shifts from its' original position as shown in Figure 15. The metacentre of the body is located at the intersection of a vertical line through the shifted centre of buoyancy and the floating bodies' centreline. The metacentric height of the pontoon, ($S/A+z_B$) is the distance between the centre of gravity and the metacentre, and is a critical quantity that determines the stability

of the pontoon in roll. If the metacentre is located lower than the centre of gravity, the floating body is unstable and will capsize.

The stiffnesses of the mooring cables were determined by catenary equations. Catenary equations must be used because the self-weight of the cables creates a non-linear force-deflection curve. A brief review of catenary equations can be found in Appendix A.

In order to reduce the motions of the bridge, the mooring cables are subject to a large pre-tension. This pre-tension varies with lake level, and is approximately equal to 500 kN when the lake is at its' the mean water level. As a result of this pre-tension, the cables have a linear force-deflection curve in the range of motion of the bridge, and can be modeled as linear springs.

The wave force time series, *F(t)* are applied at the still water level nodes. In addition, static wind loads are applied to the pontoons and the elevated road deck. Because the system is linear, the total forces and moments in the bridge can be obtained by superposing two load cases:

- the pre-tensioned system with no external loads;
- the unpre-tensioned system subject to wind and dynamic wave loads.

The natural frequencies and mode shapes of the bridge were obtained from the DSTAR module of the COSMOS/M program. The time domain dynamic analysis was performed using the ASTAR module of the program. Results of the analysis include the sway, heave and roll displacement of every node in the model, the load in the mooring cables and the bending moments about the y and z axes of the spine beam.

5. RESULTS AND DISCUSSION

5.1 DESIGN WIND AND WAVE CONDITIONS

5.1.1 DESIGN WIND SPEEDS

Wind scale factors were determined for winds from all directions and southerly and northerly winds for both Kelowna and Penticton Airports. These scale factors can be found in Table 2. The scale factors for Penticton airport were found to be lower than those for Kelowna airport. This is likely due to the fact that Penticton airport is situated close to Okanagan Lake whereas the Kelowna Airport is on a plateau above the lake. As a result, the geography and meteorology at Penticton airport more closely resembles the bridge site.

Scaled wind velocities at the bridge obtained from the Penticton airport wind record were found to be slightly larger than scaled velocities obtained from the Kelowna airport wind record. Consequently, the results obtained from the Penticton airport record have been used as design wind velocities. The 100-year design wind speeds at the Okanagan Lake Bridge corresponding to different directions and a 1-hour duration are presented in Table 3. The design wind velocity from the south is greater than the design wind velocity from the north.

5.1.2 DESIGN WAVE CONDITIONS

Design wave conditions were calculated for north and south storms with a return period of 100 years. This was accomplished by inputting the design wind velocities into MIKE 21 models of the north and south sections of Okanagan Lake. The winds were applied at 10^{o} direction intervals, and the storm durations were reduced to the minimum

required to produce fetch-limited conditions for each run. Energy dissipation due to bottom dissipation and wave breaking were not included and therefore an upper bound on wave height was calculated. The wave hindcasting results for north and south storms are presented in Tables 4 and 5 respectively. The largest wave heights and periods were obtained for the south storm, with a maximum significant wave height of 1.36 m and a corresponding peak period of 4.0 s. The maximum significant wave height obtained for the north storm was 0.83 m with a corresponding peak period of 3.2 s. The magnitude of the wave height calculated for the north storm suggests that waves are generated in the 5 km fetch immediately north of the bridge (See Figure 10).

Directional spreading indices for the north and south storms range from 3 to 4. A typical directional spreading index for an open body of water is 2, while an index value of 6 has been reported for narrow bodies of water (Hutchison and Symonds, 1986). The spreading index values calculated for Okanagan Lake appear reasonable, since the effective fetches to the north and south of the bridge are relatively broad, but not unrestricted.

5.2 STRUCTURAL AND HYDRODYNAMIC CHARACTERISTICS OF THE BRIDGE

5.2.1 HYDRODYNAMIC COEFFICIENTS

The wave diffraction program HAFB was used to obtain the hydrodynamic coefficients. The hydrodynamic coefficients include the force coefficients and phases used to create the force time series, the wave drift coefficients used to create the slowly-varying wave drift force time series, and the added masses and damping coefficients that are components of the finite element model of the bridge.

In order to calculate the hydrodynamic properties for the dynamic analysis, the program was run repeatedly with different frequency and direction waves. The force coefficients, phases and wave drift coefficients were then obtained at each frequency and direction. Added mass and hydrodynamic damping coefficients were calculated only at the peak frequency of the wave spectrum for the north and south storms. Hydrodynamic coefficients were calculated for several different pontoon geometries since the draft varies along the length of the bridge. Selected hydrodynamic coefficients for the north and south storms are presented in Tables 6 and 7 respectively.

5.2.2 NATURAL FREQUENCIES AND MODE SHAPES

The bridge is a multi-degree of freedom system, therefore numerous natural frequencies and mode shapes exist. These properties were determined through a free-vibration analysis of the bridge performed by the DSTAR module of the COSMOS/M finite element program. The analysis was performed twice since the added mass of the bridge differs for the north and south storms. Analysis of the results of the free vibration analyses reveal that the first 15 frequencies and mode shapes out of a total of 660 contribute significantly to the response of the bridge; however, 20 frequencies were included in the analysis to increase the accuracy of the results. The 20 lowest natural frequencies of the bridge are given in Tables 8 and 9 for the north and south storms respectively.

The natural periods of the bridge range from 1.37s to 15.2s for the north storm and 1.34s to 15.0s for the south storm. The north storm natural periods are greater than

the south storm natural periods due to the larger heave and roll added masses for the north storm.

5.3 BRIDGE RESPONSE FOR THE DESIGN WAVE CONDITIONS

The dynamic analysis was performed in the time domain using the ASTAR module of the COSMOS/M finite element program. The program solves the equations of motion of the bridge at each time step using Newmark's method. The time step was selected as 0.25s, or one-tenth of the period of the last mode shape that contributes significantly to the bridge response. The total number of time steps used was 5,000, which provides a simulation time of approximately 21 minutes.

The loads applied to the model included the wave force time series, slowly varying wave drift force time series and a constant wind force. The wave force time series were applied in sway, heave and roll; the slowly-varying wave drift force time series were applied only in sway. The force time series contained 250 component frequencies and 31 component directions for a total of 7,750 regular wave components. Force time series for sway, heave and roll for a 30.48 m section of the bridge in the south storm are shown in Figure 16. Force time series in sway for three adjacent sections of the bridge in the south storm are shown in Figure 17. This figure demonstrates that the wave forces on adjacent sections of the bridge are uncorrelated as expected. The slowly-varying wave drift force on a 30.48 m section of the bridge in the south storm is shown in Figure 18. This figure shows that the dynamic drift force is composed of higher frequency forces superposed on a slowly varying force, and the mean drift force is non-zero.

The COSMOS/M model was run for both north and south storms to determine the maximum response of the bridge. One wave direction was selected for the north storm and four wave directions were selected for the south storm since it was impossible to tell a priori which wave direction and height would produce the greatest bridge response.

Results of the analysis included the sway, heave and roll displacement of every node in the model, the cable tensions, and the bending moments about the y and z axes of the pontoon string. These results were obtained at every time-step of the simulation.

The maximum response of the bridge for the north and south storms for the response quantities listed above are presented in Figures 19 through 24. The displacement responses are provided at the centre of gravity of the spine beam at discrete locations along the length of the bridge. The south storm simulations provided the greatest bridge response for all response parameters.

The greatest sway and roll motions were found to occur at the east end of the bridge. The largest heave motion was found to occur near the west end of the bridge. The largest bending moment about the z-axis occurred at the east end of the bridge. As one would expect, the greatest bending moment about the y-axis was found to occur close to the centre of the bridge.

The greatest cable tensions occurred at the ends of the bridge. This is thought to be due to the fact that the shorter, and therefore stiffer cables are located at the ends of the bridge. These cables tend to carry a larger proportion of the load due their greater stiffness. The shortest south-side cable is found in the shallow water at the east end of the bridge. This cable experienced loads 28 % greater that any other cable. It may be

possible to create a more even distribution of cable loading by reducing the cross-sectional area and hence the stiffness of this cable.

5.4 BRIDGE RESPONSE FOR DIFFERENT REALIZATIONS

Time domain dynamic analysis is a sampling technique, and as a result, one can expect variability in the results. In order to ascertain the magnitude of this variability, the dynamic analysis was run 10 times for a single wave height, period and direction, with different random phases used to construct the wave force time series. The wave hindcasting results for a wave direction of 165° were selected for the input parameters.

Maximum values of the sway, heave and roll displacements, and the maximum bending moments and cable tensions obtained in each simulation are presented in Table 10; relevant statistics are presented in Table 11. The greatest variability in the results was found to occur for roll motions, with a coefficient of variation of 0.12 and a maximum difference in output parameters of 30%. The least variable results were obtained for cable tensions; however, this is largely due to the 500 kN static pre-tension in the cables. In general, the results of the investigation indicate that maximum responses cannot be obtained with confidence in a single simulation.

A potential solution to this problem is to treat the response output as a set of samples from which the population statistics must be estimated. In order to accomplish this, confidence intervals for the mean and standard deviation of the maximum responses can be constructed. The upper bound of these confidence intervals are the mean maximum response and standard deviation that are exceeded with some desired probability. Once the mean maximum responses and standard deviations have been calculated, design responses corresponding to a prescribed exceedance probability can be

derived. A detailed discussion of interval estimation theory can be found in many elementary statistics texts such as Devore (1990).

In order to construct a confidence interval for the mean of a response quantity, a set of n simulations would be performed, and the maximum of the response quantity in each simulation would be determined. The mean, $\bar{x}$ and the standard deviation, s of the maximums would then be calculated. These statistics could be calculated for the bridge as a whole or for a single node or element. If the population is assumed to be normally distributed, which is often reasonable, a confidence interval for the population mean μ, with n-1 degrees of freedom can be constructed. The 100(1-α)% confidence interval for μ is:

$$\left(\bar{x} - t_{\alpha/2,n-1} \cdot \frac{s}{\sqrt{n}}, \bar{x} + t_{\alpha/2,n-1} \cdot \frac{s}{\sqrt{n}}\right) \tag{5.1}$$

where $t_{\alpha/2,n-1}$ is the t distribution with n-1 degrees of freedom. The t distribution is a family of bell-shaped curves that are more spread out than the standard normal curve.

As the number of simulations, n increases the difference between the sample mean and standard deviation and the population mean and standard deviation generally becomes smaller. As a result, the confidence interval becomes narrower, and the upper bound of the interval becomes smaller. This phenomenon creates a trade-off between the number of simulations conducted, and the magnitude of the design response. As a result, computational effort and expense must be weighed against increased construction cost due to overestimated design forces.

A confidence interval for the standard deviation, s and variance, s^2 of a response quantity is obtained in a manner analogous to the confidence interval for the mean. The

only difference is that the chi-squared distribution is used in place of the t distribution. A 100(1-α)% confidence interval for the population variance, σ^2 can be written as follows:

$$\left(\frac{(n-1)s^2}{\chi^2_{\alpha/2,n-1}}, \frac{(n-1)s^2}{\chi^2_{1-\alpha/2,n-1}} \right) \tag{5.2}$$

where n is the number of simulations, and $\chi^2_{1-\alpha/2,n-1}$ is the chi-squared distribution with n-1 degrees of freedom. The level of confidence for both the mean and standard deviation can be set at any desired level, however, for engineering design the value would likely be 99% or greater.

Given the assumption of normality for the response output, the design response corresponding to a prescribed exceedance probability can be easily derived. The $(100p)^{th}$ percentile design response, where (1-p) is the exceedance probability of the response, can be written as follows:

$$(100p)^{th} \text{ percentile} = \mu + ((100p)^{th} \text{ percentile for the standard normal})\sigma \tag{5.3}$$

where μ and σ are the upper bounds of confidence intervals for the population mean and standard deviation respectively. The $(100p)^{th}$ percentile value for the standard normal distribution can be obtained from tables.

The technique described above was applied to the set of 10 simulations and 99% confidence intervals for the mean and standard deviation of the maximum responses were constructed. These results are presented in Tables 12 and 13. Design maximum responses corresponding to the 99^{th} percentile are presented in Table 14; the annual probability of exceedance of these responses is 10^{-4}. The Canadian Offshore Structures Code, CAN/CSA-S471-92 requires an annual exceedance probability of 10^{-2} for loads

resulting from frequent environmental processes such as waves. As a consequence, the mean maximum responses presented in Table 12 are more suitable design values.

Due to the enormous computational effort involved, confidence intervals and design responses were not calculated for the simulations described in Section 5.3. As a result, decreased confidence must be ascribed to these results.

5.5 BRIDGE RESPONSE WITHOUT SLOWLY-VARYING WAVE DRIFT FORCE

As previously mentioned, a slowly-varying wave drift force was applied to the bridge in the sway degree of freedom. In order to investigate the influence of the slowly-varying drift force, a simulation was performed with a static wave drift force. The static wave drift force was included at the significant wave height as is common in engineering practice. The random wave phases used in the simulation were identical to those used in a previous simulation. This technique effectively isolated the effect of the slowly-varying wave drift force by eliminating the random variability between runs.

The results of this simulation are presented in Table 15 along with the results of the simulation including the dynamic drift force. The simulation with the static drift force resulted in a slightly greater response for all response quantities except for bending moment about the z-axis. This is likely due to the fact that the bridge does not have low frequency natural periods in sway that may be excited by a slowly-varying force. However, the simulation does suggest that when no dynamic amplification of forces is present, a static wave drift force corresponding to the significant wave height and a slowly-varying wave drift force provide consistent results.

6. CONCLUSIONS AND RECOMMENDATIONS

6.1 CONCLUSIONS

The proposed four-lane floating bridge crossing Okanagan Lake is situated in an exposed location, and is subject to large wind and wave forces. The greatest wind velocities and largest waves were found to result from south storms. The south storm was also found to produce the largest displacements, cable tensions and bending moments in the pontoon string.

A non-negligible amount of variability was found to occur between simulations. As a consequence, a technique based on interval estimation was proposed to determine the maximum response. This technique involves performing several simulations, calculating sample statistics of the response quantities, and creating confidence intervals for the mean and standard deviation of the maximum responses. It was noted that with this technique, the magnitude of the maximum response generally becomes smaller as the number of simulations increases, and therefore an optimization problem involving computational effort and expense, and construction costs arises.

The influence of the slowly-varying wave drift force on the response of the bridge was investigated. It was determined that the slowly-varying wave drift force provided approximately the same response as a static wave drift force at the significant wave height. This result is thought to be due to the fact that the bridge does not have low frequency natural periods in sway. It is therefore recognized that a static wave drift force could be applied in order to reduce the computational effort.

State-of-the-art numerical techniques were applied to obtain the design wave conditions and perform the time domain dynamic analysis. The MIKE 21 wave hindcasting program was found to produce results generally consistent with wave data

collected at the bridge site. It is interesting to note that the wave heights and periods calculated by MIKE 21 are much lower than those obtained from less sophisticated techniques presented in the Shore Protection Manual (1984). As a result, a considerable reduction in construction costs may be realized through the use of numerical wave hindcasting techniques.

The entire numerical analysis was performed on a desktop personal computer. Computation times for numerical wave hindcasting and finite element analyses were on the order of ten minutes, while force time series generation required approximately 24 hours of processor time per simulation. Consequently, the need to perform numerous simulations may make a frequency domain approach more economical.

Perhaps the greatest advantage of the dynamic analysis technique described in this thesis is its conceptual simplicity. Creating a random, short-crested sea surface by superposing regular wave trains is more intuitive than methods based on cross-spectral densities and coherency. In addition, time domain analyses tend to be more accessible than frequency domain analyses since they are conducted in terms of tangible quantities such as forces and displacements, rather than force and response spectra. These reductions in complexity can be of considerable benefit when conducting a computationally intensive, multi-stage analysis.

6.2 RECOMMENDATIONS FOR FURTHER STUDY

There are several areas in which investigations could be made to better understand the behavior and accuracy of the solution technique described in this thesis. Firstly, the duration of the wind speeds used for wave hindcasting were 1 hour, while the simulation

time of the dynamic analysis was limited to 21 minutes due to constraints inherent in the software. Longer simulation times would likely result in higher maximum responses. It is therefore recommended that longer simulations be conducted with different structural analysis software, and that the maximum responses obtained be compared with the results of the present analysis. In addition, it is recommended that the feasibility of extrapolating the results of a 21-minute simulation to a 1-hour duration using extreme value estimation be investigated.

As discussed in Section 4.5, the frequency dependence of the hydrodynamic added mass and damping were ignored by approximating them as constant, and equal to their respective values at the peak frequency of the incident wave spectrum. This approximation was necessary since the structural analysis software could not model frequency dependent masses and dampers. The influence of this approximation on the results could be investigated by conducting a frequency domain dynamic analysis of the bridge and comparing the results with those obtained during this research.

Finally, the original intent of this thesis was to model the existing bridge, and calibrate the wave hindcasting and structural analysis results with field data collected at the bridge site. As previously mentioned, no major storm events occurred prior to the writing of the thesis and therefore calibration of the structural model with cable tension data was not possible. Furthermore, the wind and wave records collected were not of sufficient severity to permit accurate calibration of the wave hindcasting model. As a result, it is recommended that the dynamic analysis be repeated and calibrated once the ongoing field data collection program has recorded sufficient data.

NOMENCLATURE

a	= wave amplitude
A	= volume of water displaced by pontoon per unit length
$A(\omega, \theta)$	= 2-dimensional action spectrum
b	= characteristic dimension of a structure
B	= beam of pontoon segment
c, $\underline{c}$	= group velocity, group velocity vector
$\mathbf{c}$	= damping matrix
C	= force coefficient
$C(s)$	= normalizing coefficient for directional spreading function
d	= water depth
D	= difference-frequency quadratic transfer function
E, E_0, E_I	= energy source terms for action balance equation
f	= frequency
f_p	= frequency of peak of wave spectrum
F, F_D	= force exerted by a wave, wave drift force
$\mathbf{F}$	= force vector
g	= acceleration due to gravity
$G(f, \theta)$, $G(\theta)$	= directional spreading function
H, H_i	= wave height, incident wave height
H_s	= significant wave height, average height of the highest 33% of waves in a wave train
$H(f)$	= linear transfer function

k, $\underline{k}$ = wave number, $k = 2\pi/L$ where L is the wave length, stiffness, wave number vector

$\mathbf{k}$ = stiffness matrix

K_r, K_t = reflection coefficient, transmission coefficient

$m_n(\theta)$ = n^{th} moment of the action spectrum

$\mathbf{m}$ = mass matrix

n = number of simulations

p = probability

R = force reduction factor

s = directional spreading index, sample standard deviation

S = sum-frequency quadratic transfer function, moment of inertia of submerged pontoon cross section

$S(f)$ = 1-dimensional power spectrum, wave spectrum, energy spectrum

$S(f, \theta)$, $S(\omega,\theta)$ = 2-dimensional power spectrum, wave spectrum, energy spectrum

t = time, t distribution

$\mathbf{u}$ = displacement vector

V, $\underline{V}$ = wind speed, current velocity vector

x = horizontal coordinate

$\bar{x}$ = sample mean

$x(t)$ = measured realization of water surface elevation

$X(f)$ = amplitude of Fourier component

y = horizontal coordinate

z = vertical coordinate

α = parameter in JONSWAP wave spectrum, parameter in t distribution and chi-squared distribution, scale parameter in Gumbel distribution

β = scale parameter in Gumbel distribution

χ = chi-squared distribution

Δ = length of structure segment

ε = phase between force or moment and wave elevation

ϕ = phase of wave train

γ = parameter in JONSWAP wave spectrum

η = water surface elevation

μ = population mean

θ = wave direction

ρ = density of water

σ = parameter in JONSWAP wave spectrum, relative frequency for action spectrum, population standard deviation

ω = angular frequency, $\omega = 2\pi f$

BIBLIOGRAPHY

1. Barnett, T.P. 1968. On the generation, dissipation and prediction of ocean wind waves. *J. Geophys. Res.*, **73**. pp. 513-530.

2. Bathe, K.J. 1996. *Finite Element Procedures*. Prentice Hall, Upper Saddle River, New Jersey.

3. Battjes, J.A. and Janssen, J.P. 1978. Energy loss and set-up due to breaking of random waves. *Proc. 16th Coastal Engineering Conference*, Hamburg, pp. 569-587.

4. Bendat, J.S. and Piersol, A.G. 1971. *Random Data: Analysis and Measurement Procedures*. (2nd ed.). Wiley, New York.

5. Borgman, L.E. 1969. Directional spectra for design use. *Proc. Offshore Tech. Conf.*, Houston, Paper No. OTC1069, pp. 721-746.

6. Bretschneider, C.L. 1958. Revisions in wave forecasting: Deep and shallow water. *Proc. 6th Coastal Eng. Conf.*, Miami, pp. 30-67.

7. Bretschneider, C.L. 1961. A one-dimensional gravity wave spectrum. In *Ocean Wave Spectra.* Prentice-Hall, Englewood Cliffs, New Jersey, pp. 41-65.

8. Canadian Standards Association, 1992. *CAN/CSA-S471-92 Code for the design, construction, and installation of fixed offshore structures*, Toronto.

9. Cardone, V.J., Pierson, W.J. and Ward, E.G. 1976. Hindcasting the directional spectra of hurricane generated waves. *J. Petrol. Tech.*, **28**, pp. 385-394.

10. Chopra, A.K. 1995. *Dynamics of Structures: Theory and Applications to Earthquake Engineering.* Prentice Hall, Upper Saddle River, New Jersey.

11. Clough, R.W. and Penzien, J. 1993. *Dynamics of Structures*. McGraw-Hill, New York.

12. Cooley, J.W. and Tukey, J.W. 1965. An Algorithm for the machine computation of complex fourier series. *Math. Comp.*, **19**, pp. 297-301.

13. Dean, D. 1962. Static and Dynamic Analysis of Guy Cables. *ASCE Transactions,* **127**, pp. 382-419.

14. Devore, J.L. 1990. *Probability and Statistics for Engineering and the Sciences.* (3rd ed.). Brooks/Cole Publishing Company, Pacific Grove, California.

15. Engel, D.J. and Nachlinger, R.R. 1982. Frequency domain analysis of dynamic response of floating bridge to waves. *Proc. Ocean Structural Dynamics Symposium '82,* Corvalis, Oregon.

16. Fisher, R.A. and Tippett, L.H.C. 1928. Limiting forms of the frequency distribution of the largest or smallest member of a sample. *Proc. Cambridge Philosoph. Soc.*, **24**, pp. 180-190.

17. Garrison, C.J. 1969. On the interaction of an infinite shallow draft cylinder oscillating at the free surface with a train of oblique waves. *J. Fluid Mechanics*. **39**, pp. 227-255.

18. Georgiadis, C. and Hartz, B.J. 1982. A boundary element program for the computation of three dimensional hydrodynamic coefficients. *Proc. International Conference on Finite Element Methods*, Shanghai.

19. Goda, Y. 1985. *Random Seas and Design of Maritime Structures.* University of Tokyo Press, Tokyo, Japan.

20. Goldberg, L.L. 1988. In E. Lewis (Ed.). *Principles of Naval Architecture, Second Revision, Volume I, Stability and Strength.* SNAME, Jersey City, New Jersey. pp. 63-78.

21. Gumbel, E.J. 1958. *Statistics of Extremes*. Columbia Univ. Press, New York.

22. Hartz, B.J. 1981. Notes of the Spatial Correlation Factor. Appendix to a report *Okanagan Lake Bridge Dynamic Analysis*, prepared by Swan Wooster Engineering for the Ministry of Transportation and Highways, Victoria, B.C.

23. Hartz, B.J. and Georgiadis, C. 1982. A finite element program for dynamic response of continuous floating structures in short-crested waves. *Proc. International Conference on Finite Element Methods*, Shanghai.

24. Hasselmann, K. et al. 1973. Measurements of wind-wave growth and swell decay during the joint north sea wave project. *Deut. Hydrogr. Z.,* Reihe A, No. 12.

25. Hibbeler, R.C. 1995. *Structural Analysis*. (3rd. ed.). Prentice Hall, Englewood Cliffs, New Jersey.

26. Holthuijsen, L.H., Booij, N. and Herbers, T.H.C. 1989. A prediction model for stationary, short-crested waves in shallow water with ambient currents. *Coastal Engineering.* **13**, pp. 23-54.

27. Humar, J.L. 1990. *Dynamics of Structures*. Prentice Hall, Englewood Cliffs, New Jersey.

28. Hutchison, B.L. 1984. Impulse response techniques for floating bridges and breakwaters subject to short-crested seas. *Marine Technology,* **21**(3), pp. 270-276.

29. Hutchison, B.L. and Symonds, D.W. 1986. Floating bridges in short-crested random seas. *Proc. 3rd Conference on Dynamic Response of Structures*, Los Angeles.

30. Inoue, T. 1967. On the growth of the spectrum of a wind-generated sea according to a modified Miles-Phillips mechanism and its application to wave forecasting. *Tech. Rept. No. 67-5*, Geophysical Sciences Lab., New York Univ.

31. Isaacson, M., Prasad, S., Allyn, N. and Kendrick, B. 1997. Design wave loads and motions of the Okanagan Lake floating bridge. *Proc. IAHR Seminar on Multidirectional Waves and their Interaction with Structures*, San Francisco.

32. Isaacson, M. and Nwogu, O. 1987. Wave loads and motions of long structures in directional seas, *Journal of Offshore Mechanics and Arctic Engineering*, **109**(2), pp. 126-132.

33. Kim, M.H. and Yue, D.K.P. 1989. Slowly-varying wave drift forces in short-crested irregular seas. *Applied Ocean Research.* **11**(1), pp. 2-18.

34. Langen, I. and Sigbjornsson, R. 1981. Application of directional wave spectra in the evaluation of floating bridge behavior. *Proc. Specialty Conference on Directional Wave Spectra,* Berkley, California.

35. Leblanc, L., Isnard, J.L. and Wilczynski, H. 1995. A complete and consistent methodology for the assessment of mooring systems. *Proc. Offshore Technology Conference*, Houston, Paper No. OTC7709, pp. 153-164.

36. Longuet-Higgins, M.S., Cartwright, D.E., and Smith, N.D. 1961. Observations of the directional spectrum of sea waves using the motions of a floating buoy. In *Ocean Wave Spectra,* Prentice-Hall, Englewood Cliffs, N.J., pp. 111-132.

37. Longuet-Higgins, M.S. 1977. The mean forces exerted by waves on floating or submerged bodies with applications to sand bars and wave power machines. *Proc. Roy. Soc.*, London, Ser. A, **352**, pp. 463-480.

38. MacCamy, R.C. and Fuchs, R.A. 1954. Wave forces on piles: A diffraction theory. U.S. Army Corps of Engineers, *Beach Erosion Board*, Tech. Memo No. 69.

39. Marthinsen, T. 1983. The effect of short crested seas on second order forces and motions. *International workshop on ship and platform motions*. Berkley.

40. Maruo, H. 1960. The drift of a body floating on waves. *J. Ship Research*, **4**, pp. 1-10.

41. Miles, J.W. 1957-1962. On the generation of surface waves by shear flows. *JFM.* **3**, pp. 185-204. Also *JFM.* **6**, pp. 568-582; **6**, pp. 583-598; **7**, pp. 469-478; **13**, 433-448.

42. Morison, J.R., O'Brien, M.P., Johnson, J.W., and Schaaf, S.A. 1950. The forces exerted by surface waves on piles. *Petroleum Trans., AIME,* **189**, pp.149-157.

43. Newman, J.N. 1967. The drift force and moment on ships in waves. *Journal of Ship Research.* **11**, pp. 51-60.

44. Newman, J.N. 1974. Second order slowly varying forces on vessels in irregular waves. *Symp. on Dynamics of Marine Vehicles and Structures in Waves.* London.

45. Newman, J.N. 1977. *Marine Hydrodynamics*. M.I.T. Press, Massachusetts.

46. Nwogu, O.U. 1985. Wave loads and motions of long structures in directional seas. M.A.Sc. thesis, Department of Civil Engineering, University of British Columbia.

47. Pegusch, W. 1957. The Kelowna floating bridge. *The Engineering Journal.* (April). pp. 413-421.

48. Phillips, O.M. 1957. On the generation of waves by turbulent wind. *JFM.* **2**, pp. 417-445.

49. Pierson, W.J. and Moscowitz, L. 1964. A proposed spectral form for fully developed wind seas based on the similarity theory of S.A. Kitaigorodskii. J. Geophys. Res., **69**, pp. 5181-5190.

50. Pierson, W.J, Tick, L.J. and Baer, L. 1966. Computer based procedure for preparing global forecasts and wind field analysis capable of using wave data obtained from a spacecraft. *Proc. 6th Symp. Naval Hydrodynamics*, Washington, D.C.

51. Sarpkaya, T. and Isaacson, M. 1981. *Mechanics of Wave Forces on Offshore Structures.* Van Nostrand Reinhold, New York.

52. Svendsen, I.A. and Jonsson, I.G. 1980. *Hydrodynamics of Coastal Regions*. Den Private Ingeniorfond, Lyngby, Denmark.

53. Sverdrup, H.U. and Munk, W.H. 1947. Wind, sea and swell; Theory of relations for forecasting. *U.S. Navy Hydrogr. Office*, Pub. No. 601.

54. Ursell, F. 1949. On the heaving motion of a circular cylinder on the surface of a fluid. *Quart. J. Mech. Appl. Math.* **2**, pp. 218-231.

55. U.S. Army, Coastal Engineering Research Center. 1984. *Shore Protection Manual.* Vicksburg, Mississippi.

56. Vugts, J.H. 1968. The hydrodynamic coefficients for swaying, heaving and rolling cylinders in a free surface. *Int. Shipbuilding Prog.,* **15**, pp. 251-276.

APPENDIX A

CATENARY EQUATIONS

The following review of catenary equations is from Dean (1962). Consider an element of perfectly flexible cable with length *ds* as shown in (A1) 1A. The cable is subject to a horizontal force *H*, and has unit weight *q*. A sum[illegible] of vertical forces yields the differential equation of the cable curve:

(A2)

(A3)

This differential equation can be solved to yield the fol[illegible] solution and integration constant:

(A4)

(A5)

where $r = ql/2H$. The cable tension, *T* at any poin[illegible] ven by the following equation:

A key relation which relates the total cable length, L to the other variables is as follows:

Thus, if the geometry of the cable endpoints and the horizontal force in the cable are known, the length of the cable can be calculated. When this quantity is known, the horizontal force in the cable can be calculated for different endpoint geometries. In this manner, a force deflection curve for the cable can be created.

The equations presented above can be further refined by accounting for the elastic stretch of the cable through integration over the cable length.

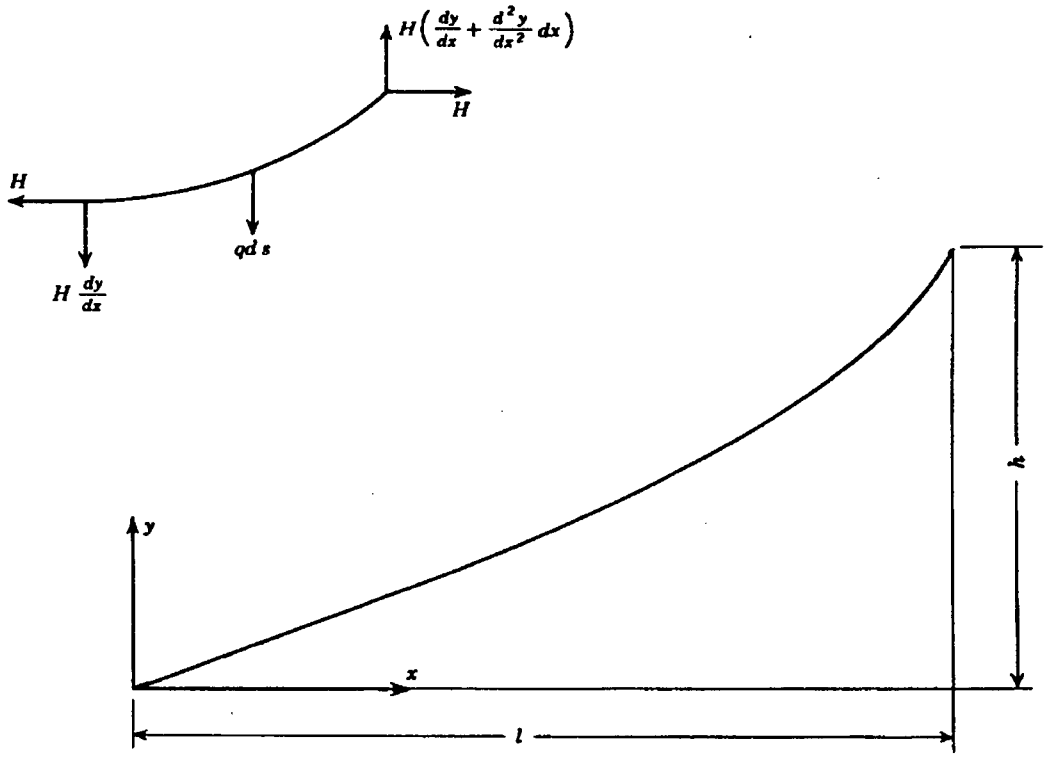

Figure 1A. Definition sketch of hanging cable and element (Dean, 1962).

Table 1. Comparison of measured wave heights and wave periods and those calculated by the MIKE 21 wave hindcasting computer program for south storms (July 1998 to March 1999).

Measured				MIKE 21		Percent Difference	
Wind Speed (km/hr)	**Direction (degrees)**	**H_s(m)**	**T_p(s)**	**H_s(m)**	**T_p(s)**	**H_s(m)**	**T_p(s)**
39.0	207	0.28	3.1	0.41	2.7	31.4	-13.4
39.0	207	0.29	2.9	0.41	2.7	29.5	-6.0
35.2	190	0.34	2.9	0.37	2.6	8.1	-11.1
35.2	190	0.38	2.9	0.37	2.6	-5.0	-11.1
35.2	190	0.41	3.1	0.37	2.6	-11.2	-18.8
38.8	233	0.30	2.9	0.35	2.5	14.0	-16.7
38.8	233	0.34	3.0	0.35	2.5	5.0	-20.7
38.8	233	0.34	3.0	0.35	2.5	5.0	-20.7
37.2	232	0.34	2.9	0.33	2.5	-1.7	-16.7
37.2	232	0.34	3.1	0.33	2.5	-3.1	-24.7
42.1	228	0.28	3.1	0.4	2.6	29.3	-18.8
42.1	228	0.32	3.1	0.4	2.6	20.9	-18.8
33.5	221	0.33	2.9	0.32	2.5	-1.8	-16.7
33.5	221	0.30	3.0	0.32	2.5	6.2	-20.7

Table 2. Wind speed scaling factors for Penticton and Kelowna airports.

Direction	**Scaling Factor**	
	Penticton Airport	**Kelowna Airport**
All	1.11	1.39
Northerly	1.18	1.20
Southerly	1.09	1.50

Table 3. Design 100-year wind speeds for a 1-hour duration storm.

Direction	100 Year Wind (km/hr)
All	112.7
Northerly	86.7
Southerly	105.3

Table 4. Wave hindcasting results for the 100-year south storm.

Wind Direction (degrees)	Wind Speed (m/s)	H_s (m)	T_p (s)	Spreading Index, s
215	28.5	1.29	3.9	3.5
205	28.8	1.35	4.0	4.0
195	28.8	1.36	4.0	4.0
185	29.2	1.36	4.0	4.0
175	29.2	1.33	4.0	4.0
165	29.2	1.29	4.0	4.0

Table 5. Wave hindcasting results for the 100-year north storm.

Wind Direction (degrees)	Wind Speed (m/s)	H_s (m)	T_p (s)	Spreading Index, s
350	24.1	0.83	3.2	4.0
0	22.8	0.75	3.1	4.0
10	22.8	0.72	3.1	4.0
20	22.8	0.64	2.9	3.0

Table 6. Selected hydrodynamic coefficients for the south storm.

Hydrodynamic Coefficient	Degree of Freedom		
	Sway	Heave	Roll
Force	0.368	0.523	0.186
Phase	189.9°	193.4°	189.6°
Added Mass	0.048	1.812	0.313
Damping	0.139	0.299	0.037
Drift Force	0.484	0.0	0.0

Table 7. Selected hydrodynamic coefficients for the north storm.

Hydrodynamic Coefficient	Degree of Freedom		
	Sway	Heave	Roll
Force	0.324	0.312	0.102
Phase	104.3°	100.6°	105.4°
Added Mass	0.022	1.980	0.327
Damping	0.103	0.118	0.012
Drift Force	0.497	0.0	0.0

Notes:

1) Hydrodynamic coefficients presented are for a pontoon with a 2.5 m draft at the centre of the bridge.
2) The force coefficients are for waves approaching the bridge at 90° to the bridge axis.
3) The force coefficients are defined as:
   - Sway, Heave: (Force per unit length)/(a*ρ*g*b)
   - Roll: (Moment per unit length)/(a*ρ*g*b^2)
   - Drift: (Force per unit length)/(a*a*ρ*g)
4) The added mass coefficients are defined as:
   - Sway, Heave: (Added mass per unit length)/(ρ*b^2)
   - Roll: (Added mass per unit length)/(ρ*b^4)
5) The damping coefficients are defined as:
   - Sway, Heave: (Damping per unit length)/(ρ*ω*b^2)
   - Roll: (Damping per unit length)/(ρ*ω*b^4)
6) In the preceding definitions, a is the wave amplitude, ρ is the density of water, g is the acceleration due to gravity, b is a characteristic length set at 10 m, and ω is the peak period of the storm in radians/second.
7) ω is equal to 1.57 radians/second for the south storm and 1.96 radians/second for the north storm.

Table 8. Natural frequencies and periods of the bridge for the south storm.

Frequency Number	Frequency (Hz)	Period (s)
1	0.067	15.0
2	0.127	7.84
3	0.131	7.61
4	0.145	6.89
5	0.151	6.62
6	0.154	6.48
7	0.171	5.84
8	0.187	5.35
9	0.210	4.77
10	0.220	4.54
11	0.268	3.73
12	0.330	3.03
13	0.344	2.90
14	0.367	2.73
15	0.434	2.30
16	0.549	1.82
17	0.639	1.56
18	0.653	1.53
19	0.694	1.44
20	0.744	1.34

Table 9. Natural frequencies and periods of the bridge for the north storm.

Frequency Number	Frequency (Hz)	Period (s)
1	0.066	15.2
2	0.123	8.14
3	0.131	7.66
4	0.141	7.07
5	0.149	6.72
6	0.153	6.52
7	0.166	6.02
8	0.189	5.29
9	0.204	4.91
10	0.222	4.51
11	0.261	3.83
12	0.328	3.04
13	0.335	2.98
14	0.370	2.70
15	0.422	2.37
16	0.534	1.87
17	0.639	1.56
18	0.645	1.55
19	0.692	1.44
20	0.731	1.37

Table 10. Summary of results of 10 simulations of a south storm.

Simulation Number	Heave (m)	Sway (m)	Roll (degrees)	Y-axis Bending Moment (kNm)	Z-axis Bending Moment (kNm)	Cable Tension (kN)
1	0.193	0.304	0.507	216000	177600	1318
2	0.244	0.362	0.498	245900	179600	1520
3	0.182	0.264	0.460	183500	162000	1257
4	0.178	0.348	0.490	216900	175800	1488
5	0.199	0.321	0.605	201700	163200	1367
6	0.186	0.338	0.509	217200	173900	1507
7	0.216	0.344	0.659	256900	198900	1396
8	0.196	0.345	0.523	217600	197400	1543
9	0.201	0.329	0.463	225600	206900	1436
10	0.195	0.289	0.509	209300	161400	1255

Table 11. Statistics obtained from 10 simulations of a south storm.

Response Quantity	Average	Standard Deviation	Coefficient of Variation	Maximum	Minimum	Maximum Percentage Difference
Heave (m)	0.199	0.0191	0.096	0.244	0.178	27.1
Sway (m)	0.324	0.0304	0.095	0.361	0.264	27.1
Roll (degrees)	0.522	0.0624	0.12	0.659	0.460	30.3
Y-axis Bending Moment (kNm)	219069	20746	0.095	256900	183533	28.6
Z-axis Bending Moment (kNm)	179672	16313	0.091	206900	161400	22.0
Cable Tension (kN)	1409	107	0.076	1543	1255	18.7

Table 12. Upper and lower bounds of 99% confidence intervals for the mean maximum response of the bridge.

Response Quantity	Lower Bound	Upper Bound
Heave (m)	0.179	0.219
Sway (m)	0.293	0.355
Roll (degrees)	0.458	0.586
Y-axis Bending Moment (kNm)	197747	240391
Z-axis Bending Moment (kNm)	162906	196437
Cable Tension (kN)	1298	1519

Table 13. Upper and lower bounds of 99% confidence intervals for the standard deviation of the maximum response of the bridge.

Response Quantity	Lower Bound	Upper Bound
Heave (m)	0.012	0.043
Sway (m)	0.019	0.069
Roll (degrees)	0.039	0.142
Y-axis Bending Moment (kNm)	12815	47251
Z-axis Bending Moment (kNm)	10076	37154
Cable Tension (kN)	66.4	244

Table 14. Design values for the maximum response of the bridge with an annual exceedance probability of 10^{-4}.

Response Quantity	Design Response
Heave (m)	0.320
Sway (m)	0.517
Roll (degrees)	0.917
Y-axis Bending Moment (kNm)	350487
Z-axis Bending Moment (kNm)	283009
Cable Tension (kN)	2090

Table 15. Comparison of results obtained with static and dynamic wave drift forces applied to the bridge.

Response Quantity	Dynamic Drift Force	Static Drift Force	Percentage Difference
Heave (m)	0.193	0.194	-0.35
Sway (m)	0.304	0.309	-1.68
Roll (degrees)	0.507	0.543	-7.02
Y-axis Bending Moment (kNm)	216049	222400	-2.94
Z-axis Bending Moment (kNm)	177560	177500	0.03
Cable Tension (kN)	1318	1328	-1.17

Figure 1. The Bergsoysundet Floating Bridge in Norway. An example of an arched floating bridge.

Figure 2. The First and Third Lake Washington Floating Bridges in Seattle, Washington, USA. An example of floating bridges given lateral support by mooring cables.

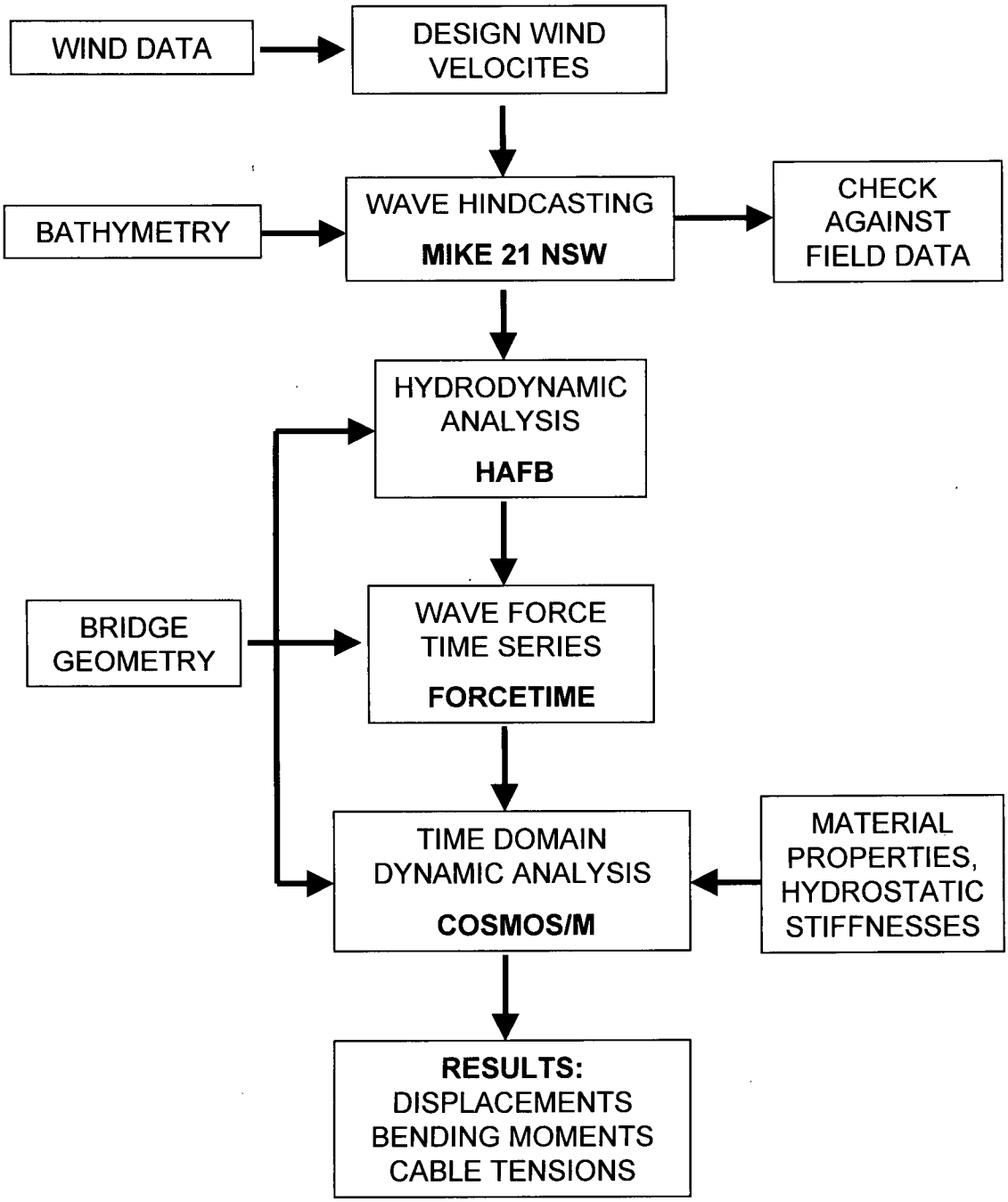

Figure 3. Flow chart for the dynamic analysis of the Okanagan Lake Floating Bridge.

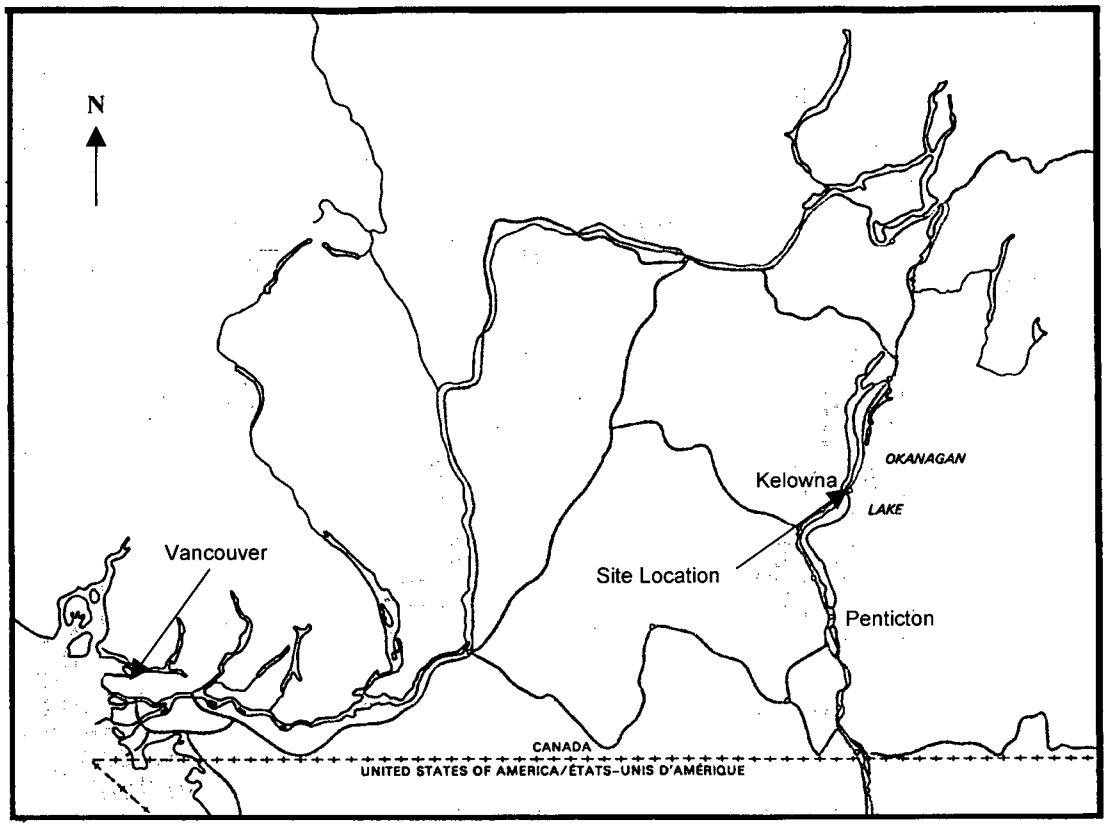

Figure 4. Location of the Okanagan Lake Floating Bridge, in Kelowna, British Columbia, Canada.

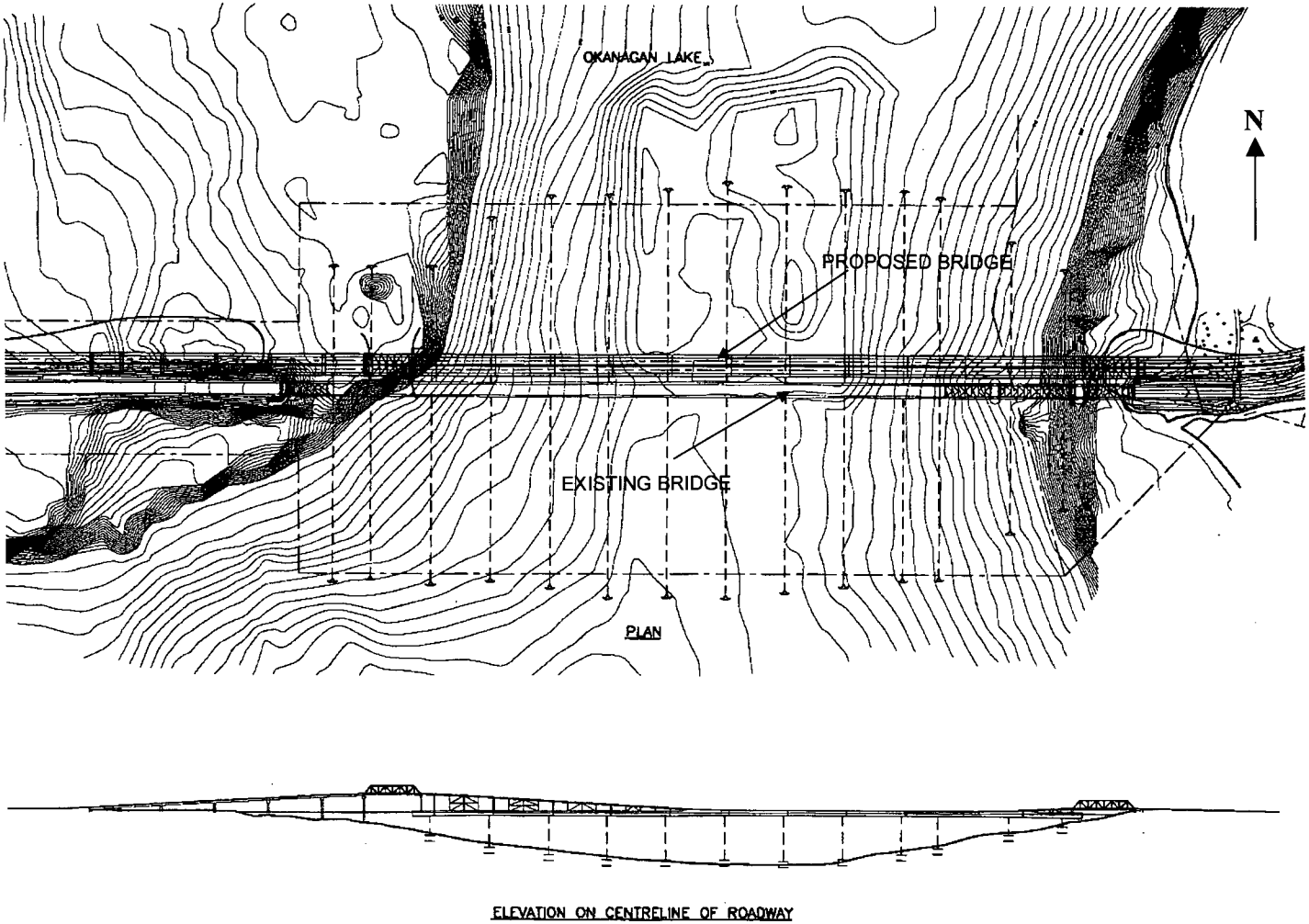

Figure 5. Plan and elevation views of the proposed four-lane floating bridge in Kelowna, British Columbia, Canada. The existing bridge is south of the proposed bridge.

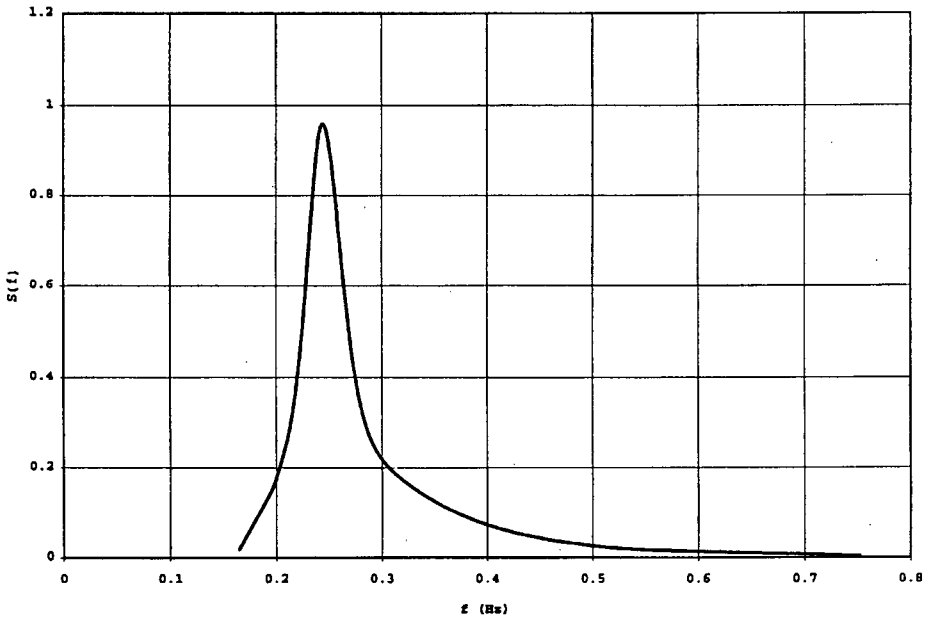

Figure 6. An example of a JONSWAP wave spectrum.

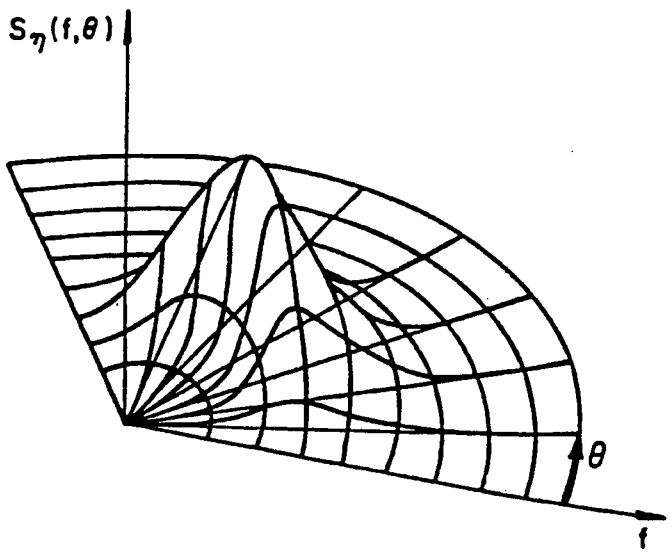

Figure 7. An example of a directional wave spectrum (Sarpkaya and Isaacson, 1981).

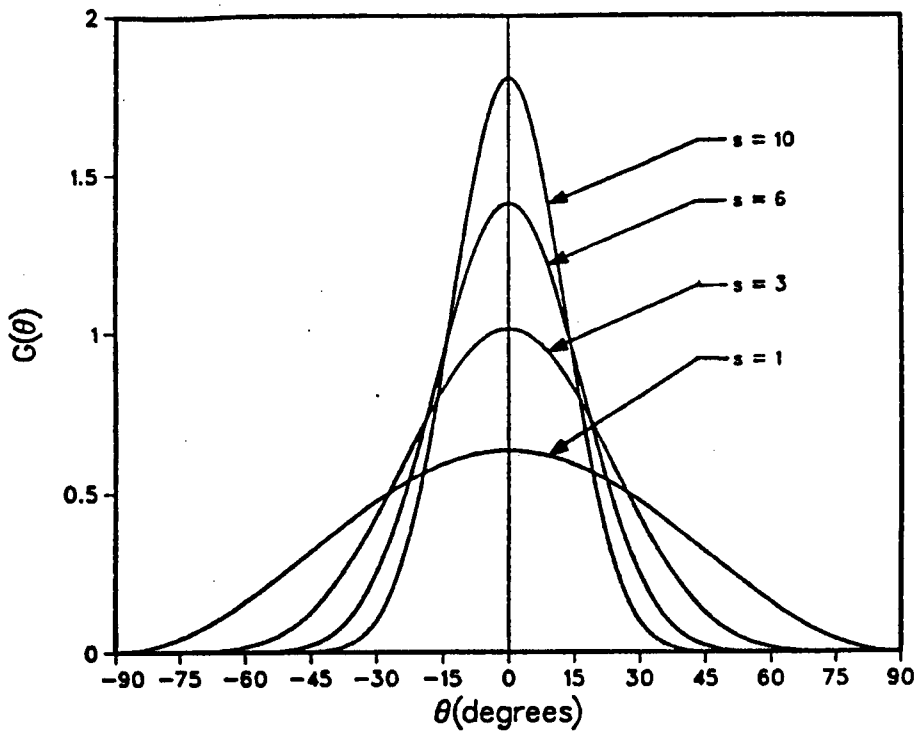

Figure 8. A cosine power directional spreading function for various values of the directional spreading index, s (Sarpkaya and Isaacson, 1981).

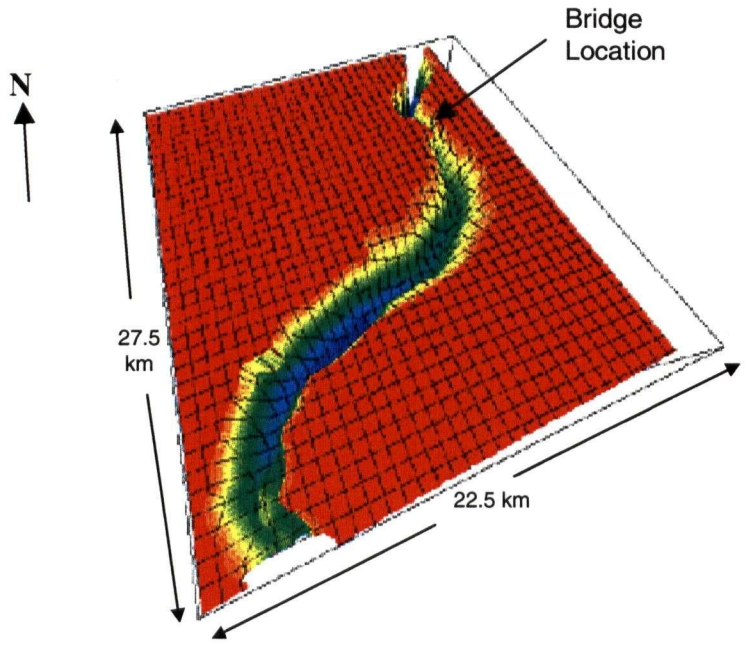

Figure 9. 3-Dimensional view of the bathymetry of Okanagan Lake to the south of the bridge site used in the MIKE 21 numerical wave hindcasting model.

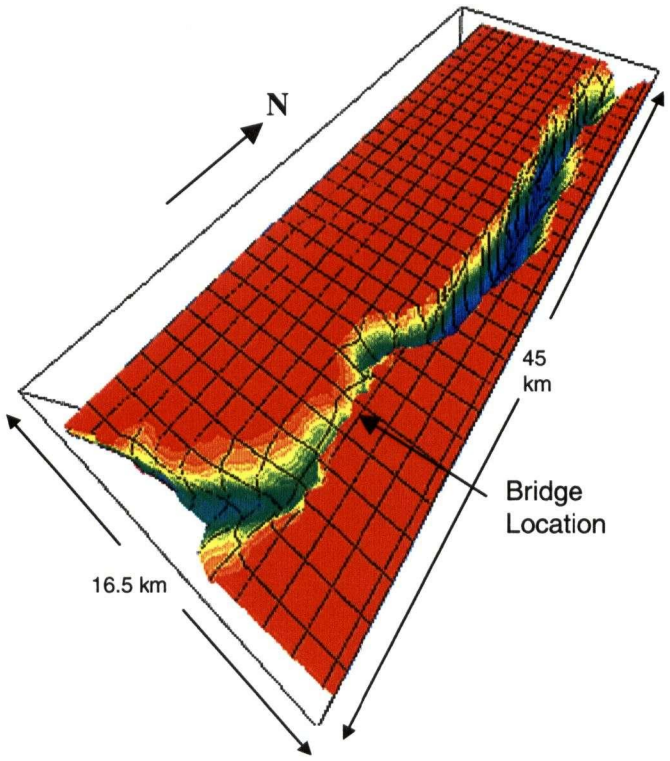

Figure 10. 3-Dimensional view of the bathymetry of Okanagan Lake to the north of the bridge site used in the MIKE 21 numerical wave hindcasting model.

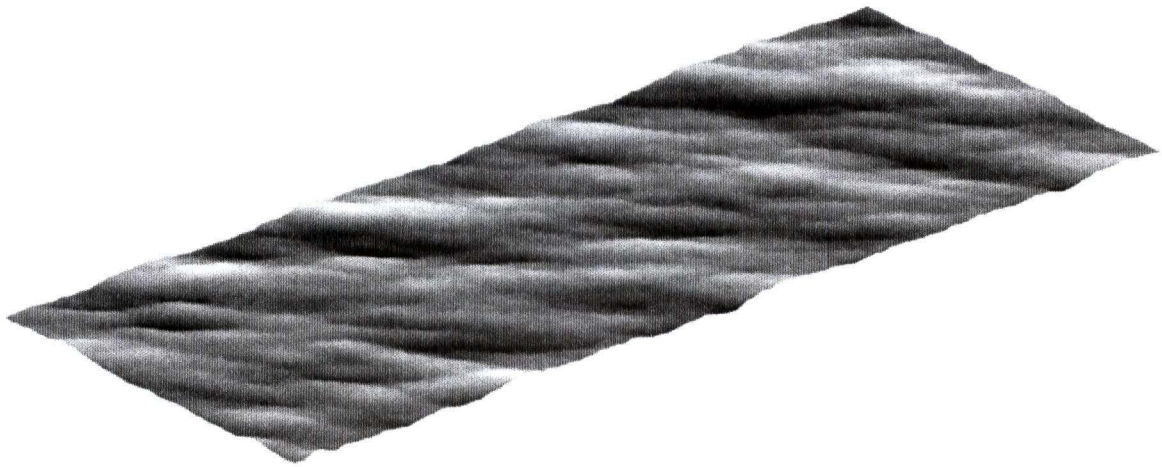

Figure 11. Short-crested wave field produced by Equation 4.5.

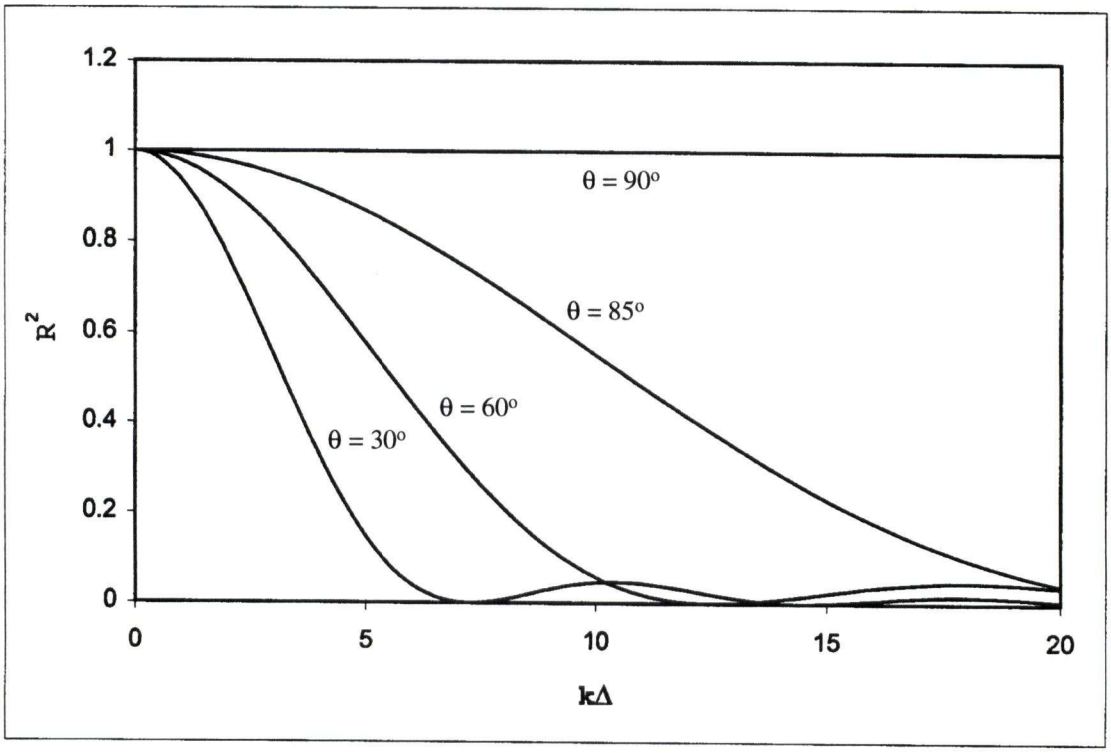

Figure 12. The square of the force reduction factor, R as a function of kΔ for various values of incident wave angle, θ.

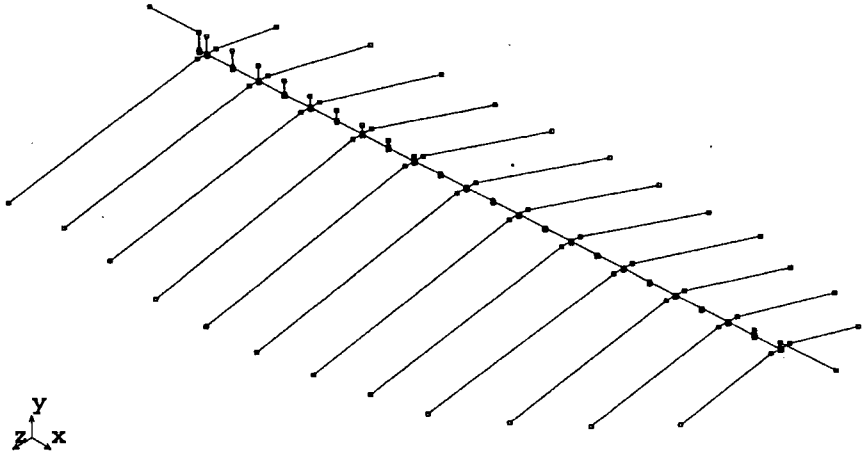

Figure 13. Isometric view of the COSMOS/M finite element model of the bridge.

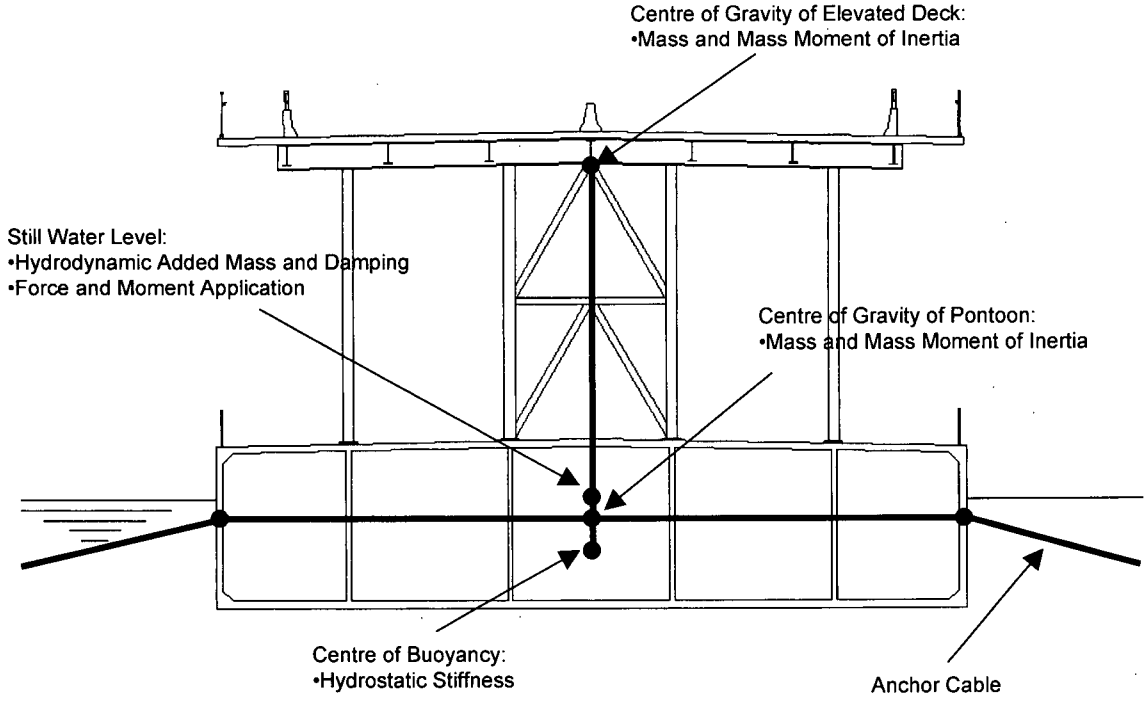

Figure 14. Cross-sectional view of the COSMOS/M finite element model of the bridge showing mass, spring and damper locations.

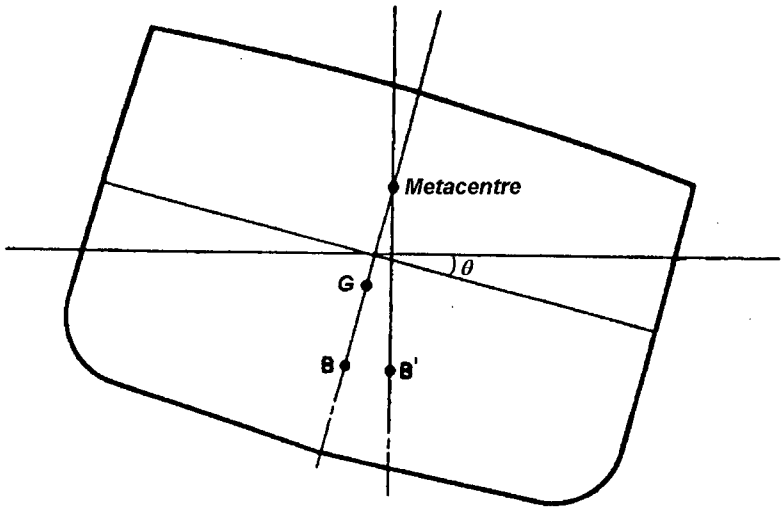

Figure 15. Shift of the centre of buoyancy, B and location of the metacentre of a rolling floating body.

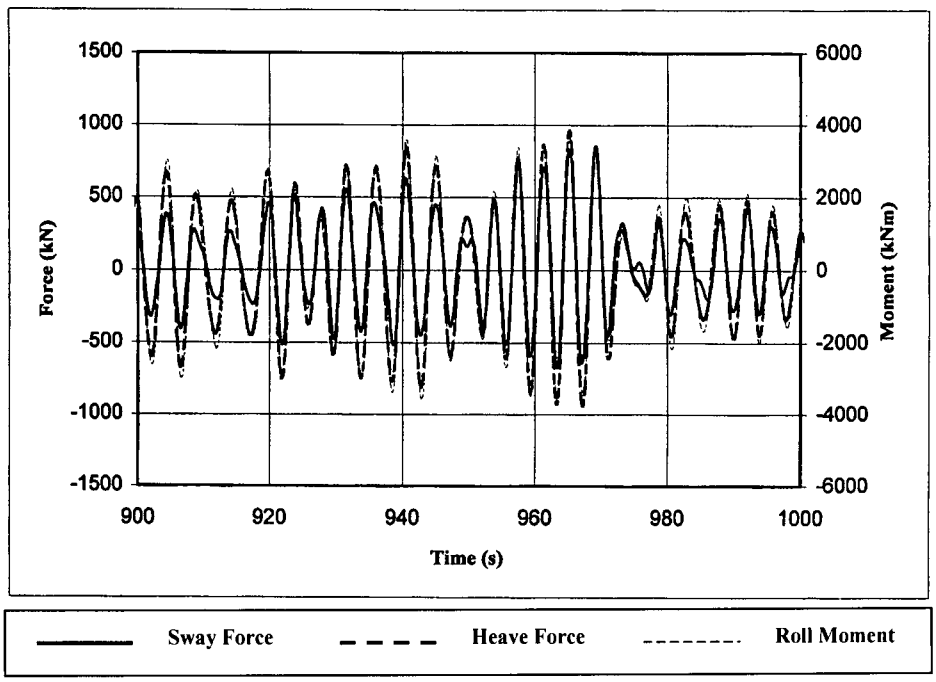

Figure 16. Sway and heave force, and roll moment applied to a 30.48 m section of the bridge during a south storm.

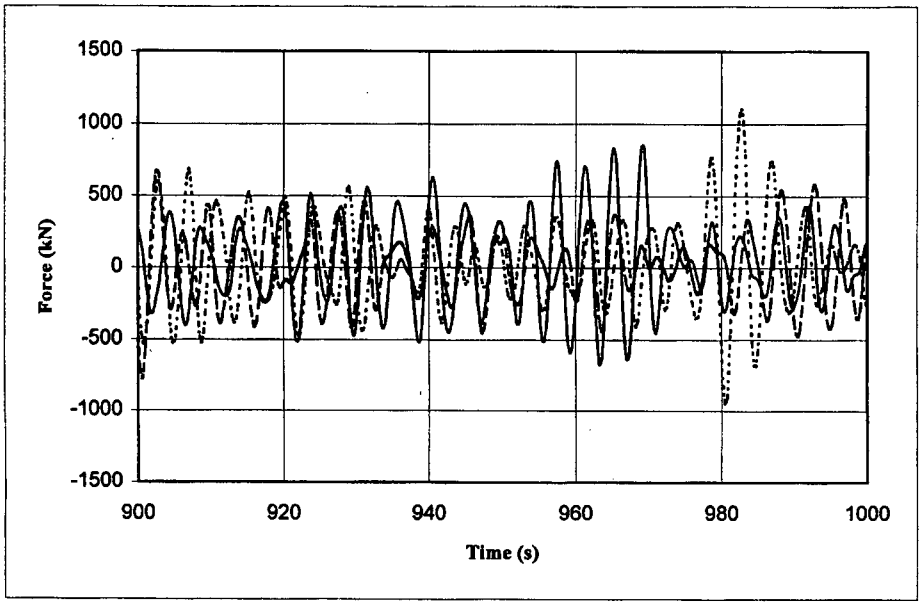

Figure 17. Sway force applied to three adjacent 30.48 m sections of the bridge during a south storm.

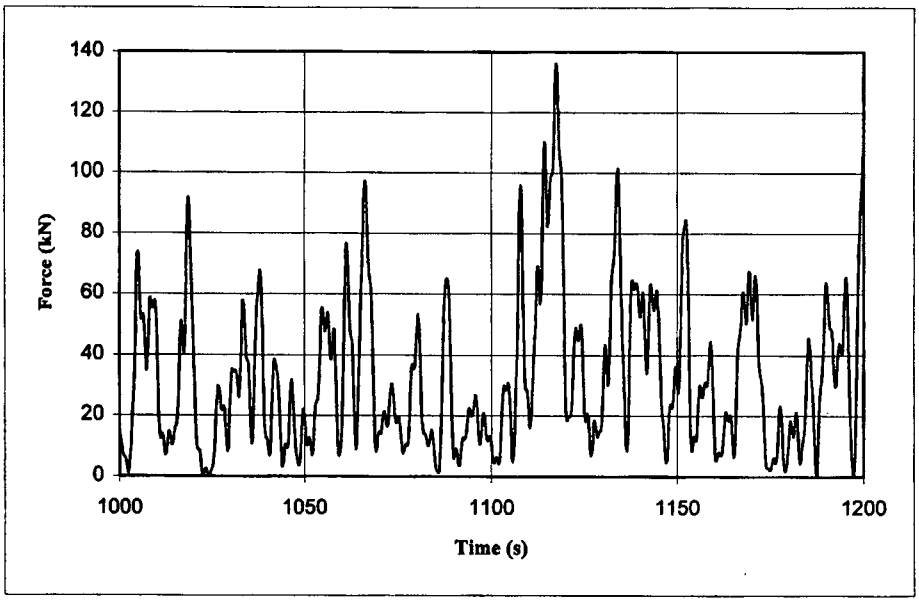

Figure 18. Slowly-varying wave drift force applied to a 30.48 m section of the bridge during a south storm.

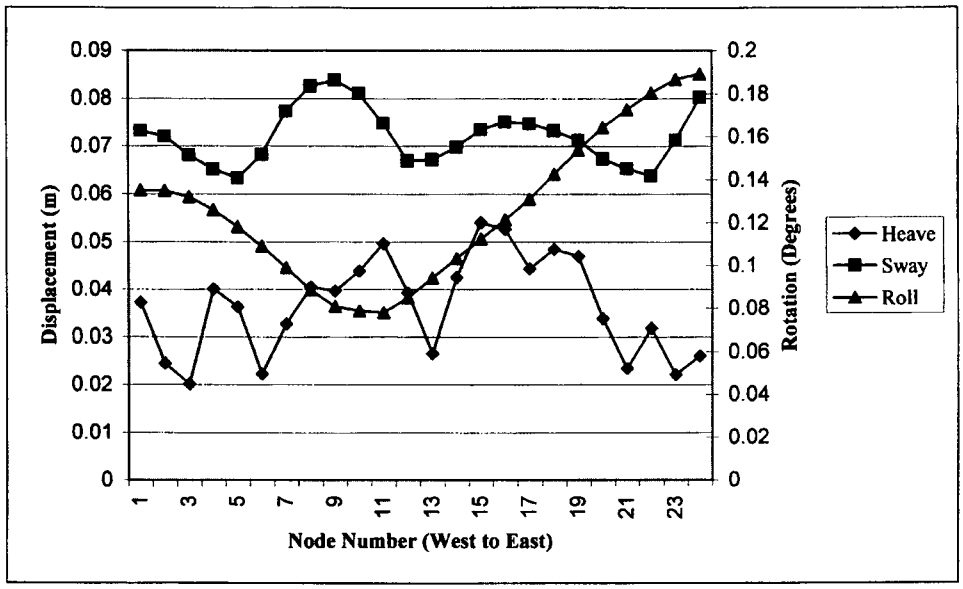

Figure 19. Maximum sway, heave and roll displacements along the bridge span during the north storm.

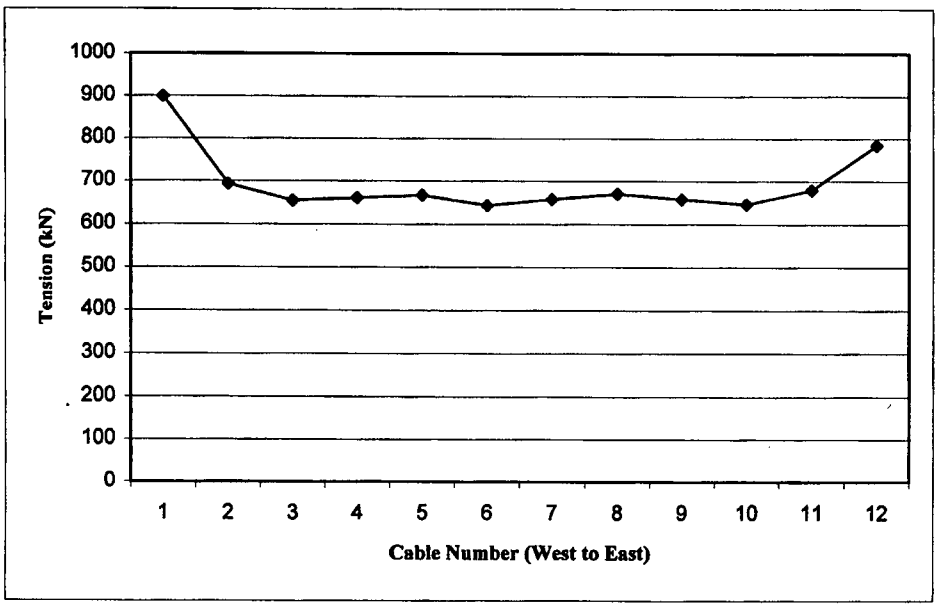

Figure 20. Maximum cable tensions (including static pre-stress) along the bridge span during the north storm.

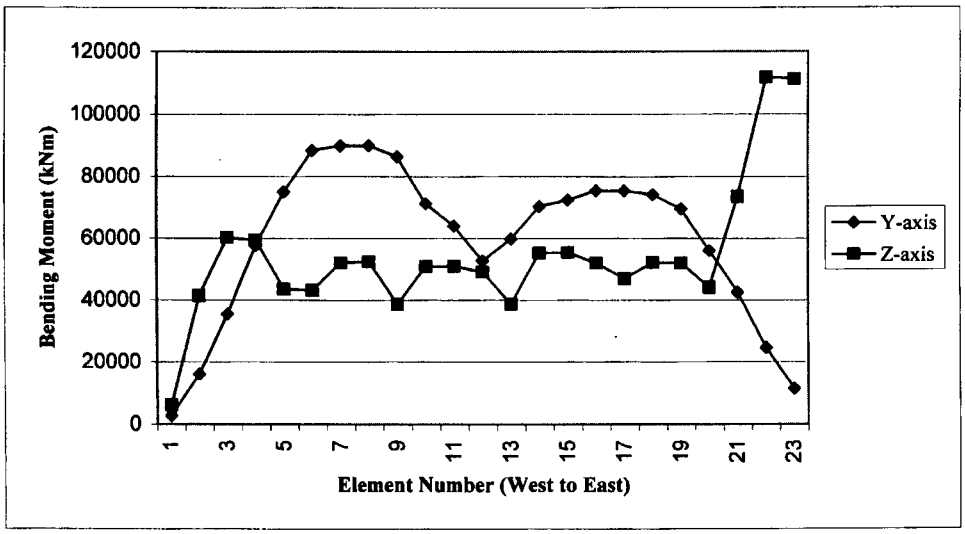

Figure 21. Maximum bending moments about the y and z axes of the pontoon string during the north storm.

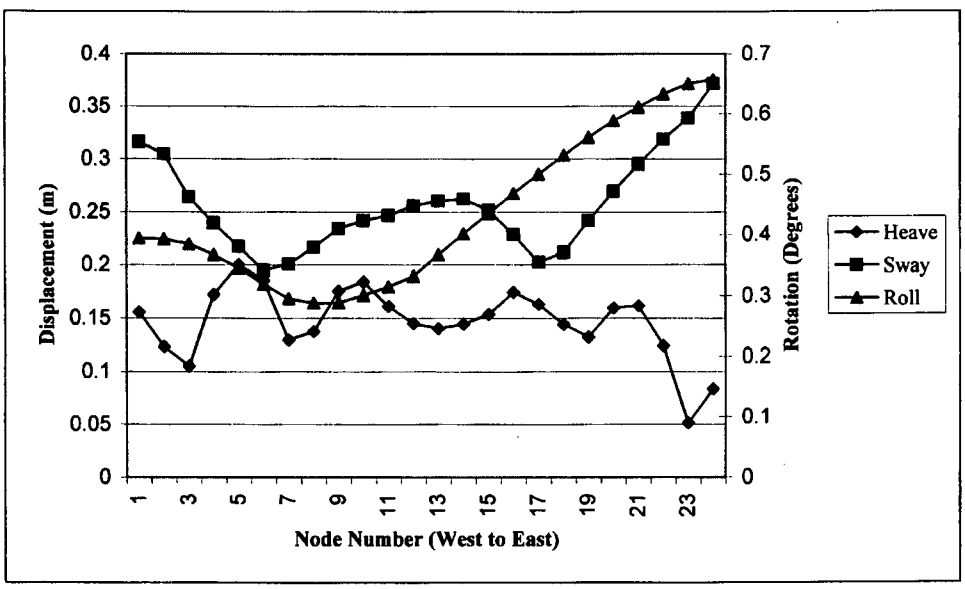

Figure 22. Maximum sway, heave and roll displacements along the bridge span during the south storm.

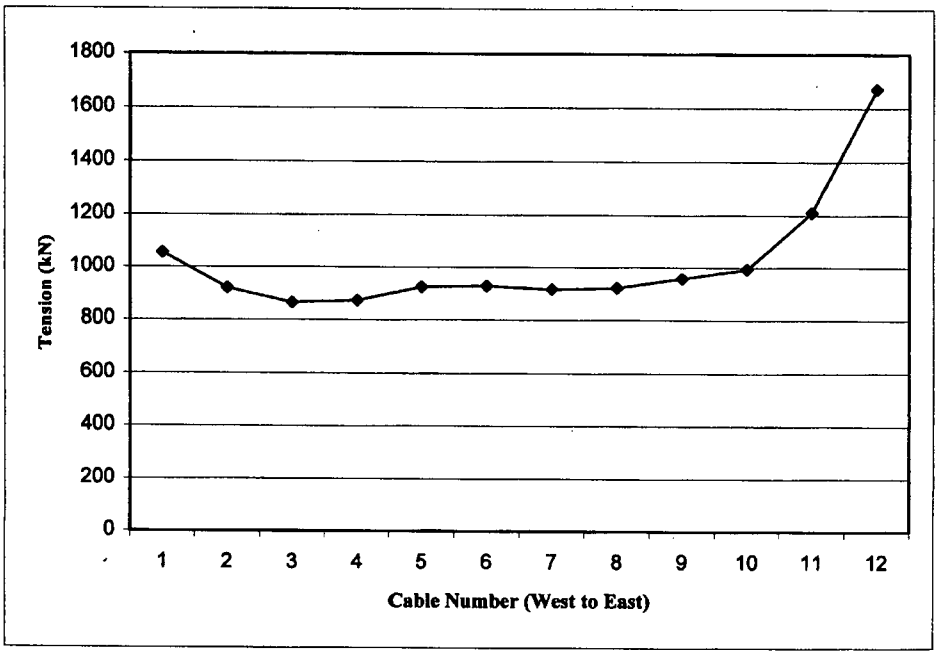

Figure 23. Maximum cable tensions (including static pre-stress) along the bridge span during the south storm.

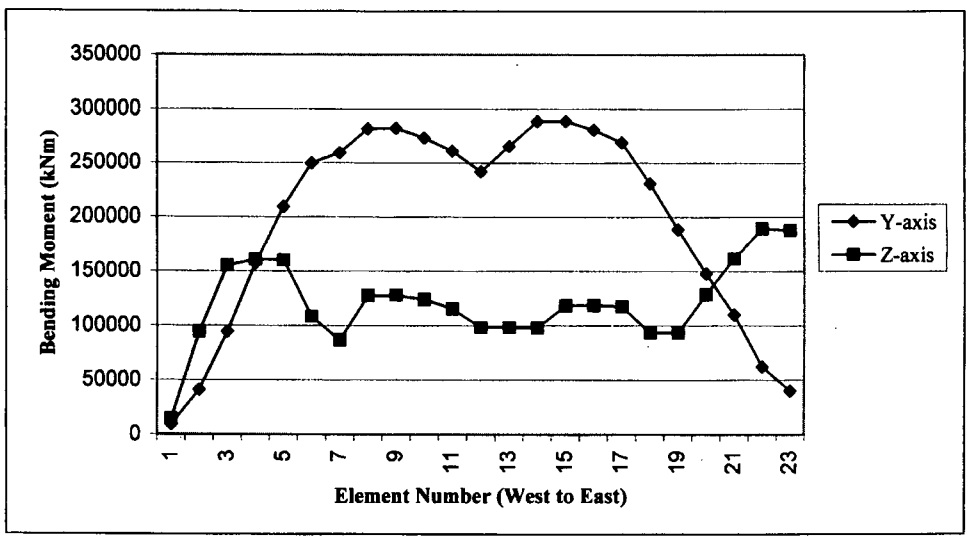

Figure 24. Maximum bending moments about the y and z axes of the pontoon string during the south storm.